




Review

Review of Auxetic Materials for Sports Applications: Expanding Options in Comfort and Protection

Olly Duncan ¹, Todd Shepherd ², Charlotte Moroney ³, Leon Foster ⁴ ,
Praburaj D. Venkatraman ³, Keith Winwood ^{2,5}, Tom Allen ²  and Andrew Alderson ^{1,*} 

¹ Materials and Engineering Research Institute, Sheffield Hallam University, Sheffield S1 1WB, UK; Oliver.H.Duncan@student.shu.ac.uk

² Sports Engineering Research Team, Manchester Metropolitan University, Manchester M1 5GD, UK; todd.shepherd@stu.mmu.ac.uk (T.S.); k.winwood@mmu.ac.uk (K.W.); T.Allen@mmu.ac.uk (T.A.)

³ Manchester Fashion Institute, Manchester Metropolitan, Manchester M15 6BH, UK; charlotte.m.moroney@stu.mmu.ac.uk (C.M.); p.venkatraman@mmu.ac.uk (P.D.V.)

⁴ Centre for Sports Engineering Research, Sheffield Hallam University, Sheffield S1 1WB, UK; l.i.foster@shu.ac.uk

⁵ School of Healthcare Science, Manchester Metropolitan University, Manchester M1 5GD, UK

* Correspondence: a.alderon@shu.ac.uk; Tel.: +44-(0)-114-225-3523

Received: 10 May 2018; Accepted: 31 May 2018; Published: 6 June 2018



Abstract: Following high profile, life changing long term mental illnesses and fatalities in sports such as skiing, cricket and American football—sports injuries feature regularly in national and international news. A mismatch between equipment certification tests, user expectations and infield falls and collisions is thought to affect risk perception, increasing the prevalence and severity of injuries. Auxetic foams, structures and textiles have been suggested for application to sporting goods, particularly protective equipment, due to their unique form-fitting deformation and curvature, high energy absorption and high indentation resistance. The purpose of this critical review is to communicate how auxetics could be useful to sports equipment (with a focus on injury prevention), and clearly lay out the steps required to realise their expected benefits. Initial overviews of auxetic materials and sporting protective equipment are followed by a description of common auxetic materials and structures, and how to produce them in foams, textiles and Additively Manufactured structures. Beneficial characteristics, limitations and commercial prospects are discussed, leading to a consideration of possible further work required to realise potential uses (such as in personal protective equipment and highly conformable garments).

Keywords: injury; impact; indentation; comfort; protective equipment; negative Poisson's ratio; foam; textiles; Additive Manufacturing; finite element modelling; auxetic

1. Introduction

Auxetic materials have a negative Poisson's ratio (NPR) [1], meaning they expand laterally in one or more perpendicular direction/s when they are extended axially. Poisson's ratio (ν) is the negative of the ratio of lateral to axial strain (Figure 1). The potential application of foams, textiles and additively manufactured (AM) auxetic materials to sporting protective equipment (PE), as well as other forms of impact protection, has been discussed in articles with a focus on materials (e.g., [2–5]) and sport (e.g., [6–8]). Auxetic foam was the first man made auxetic material [9], and makes up a significant proportion of the scientific literature and therefore this review. Foam studies typically use relatively established fabrication methods for auxetic polyurethane (PU) foams, with tests often based upon those outlined in standards used to certify sports safety equipment (i.e., British Standards

Institution—BSI, International Organization for Standardization—ISO, American Society for Testing and Materials—ASTM). Idealised structures (e.g., those fabricated via AM) and textiles can be designed to have repeat patterns that provide NPR in either one or two planes [5].

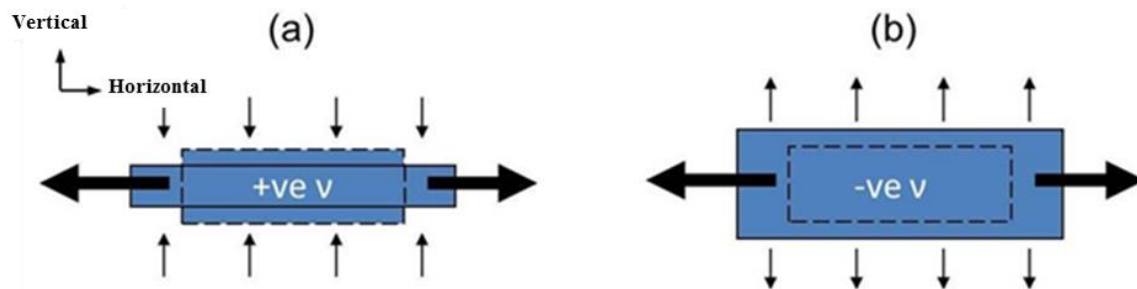


Figure 1. Lateral (vertical) deformation due to Poisson's ratio during tensile axial (horizontal) loading for (a) a conventional material and (b) an auxetic material. Thick and thin arrows correspond to deformation due to loading and Poisson's ratio respectively.

There are numerous reviews into auxetic materials and/or structures [10–17], but there has not yet been one focussing on their application to sporting goods. Deficiencies in standards (or a lack of a standard in some instances) and PE [18,19] indicate changes in equipment testing and design are likely, with the need for novel and improved materials to meet new requirements.

Recent developments in the fabrication of auxetic PU foam have deepened our understanding of the mechanisms that can fix an imposed cell structure, while improving and diversifying fabrication methods. Developments include rapid fabrications [20,21] and the ability to tailor elastic modulus and Poisson's ratios of anisotropic and gradient foam samples [22,23]. Finite element modelling (FEM) has been applied to auxetic materials [24–26] but has not been fully explored to support their implementation within sports equipment. With developments in AM [27], the creation of idealised auxetic structures (computationally tested using FEM) has become commercially viable [28]. Developing fabrication techniques for auxetic textiles and composites are also bringing both protective and form-fitting auxetic garments closer to realisation [29].

The focus of this review is on sports equipment and auxetic materials, predominantly auxetic foams, textiles and FEM/AM for impact protection. NPR can provide uniquely high indentation resistance [30,31] and fracture toughness [32], lending auxetic materials well to impact force or acceleration attenuating scenarios, regularly demonstrated by impacting auxetic foams [2,3,33]. Auxetics' multi-axial expansion [34,35] and double curvature [9,36,37] could improve comfort, fit and durability in sporting garments and personal protective equipment (PPE). Multi-axial expansion could also be useful in filtration applications [9,38–40], while gradient structures' enhanced bending stiffness [41,42] could reduce the mass of skis, snowboards, tennis rackets or hockey sticks (to name a few), without sacrificing stiffness. An initial summary of current sporting PE and PPE will lead to descriptions of common auxetic structures and materials, how to create them and how they could resolve issues in sporting PE, PPE, garments and other sports equipment.

2. Introduction to Sporting Protective Equipment

Injuries in sport are common and place a significant burden upon participants and national economies [43,44], estimated at \$525 (~£380) million per year in The Netherlands [45] for example. The main methods of intervention are elimination, modification (a reduction in severity or likelihood of injury) and reaction (i.e., medical) [44]. Preventative measures such as sports safety equipment, and/or rule changes, are more cost effective than reactive procedures [44] and successful products can increase a manufacturer's share of the sporting goods market (~\$90/£66 billion in the USA in 2017 [46]). Sporting PE is intended to reduce risks and is typically either an addition to the playing field or environment (i.e., crash matt or barrier, known herein as PE) or PPE. Both equipment

types provide; (i) protection against impact, dissipating and absorbing energy while reducing peak forces/accelerations, pressures and in some cases such as helmets, impulses [43,44,47–49] and (ii) protection from penetration, abrasions and lacerations [18,47,48,50]. Sporting PPE can also provide support to joints, muscles and the skeleton [18,44,47,48,51].

Sporting PPE (Figure 2a) often contains a shell—typically a stiff material or non-Newtonian fluid layer—to spread forces and reduce pressures [47,48,50,52]. Impacts are typically attenuated by elastic [44,52], viscoelastic and/or permanent deformation (i.e., crushable foam in cycling helmets) of a cushioning material with a lower compressive stiffness than the shell [47,48,50,52]. Visco-elastic and permanent deformation reduce impulses, improving the level of protection [44].

Sporting PPE must sometimes cover large areas and should ideally be low in mass and bulk to reduce restriction of movement, fatigue and heat build-up. Foam is typically used for the cushioning layer in PPE, and with limited thickness to compress and decelerate impacting bodies material selection is crucial. In contrast, PE such as crash mats (where bulk, mass and ergonomics are less critical) are often large and thick, allowing more gradual deceleration over a greater distance through compression of relatively compliant foam [52]. For both sporting PE and PPE, deceleration (or force) ideally reaches a maximum yet safe value at low strains, before plateauing and deforming with no additional load to safely maximise energy absorption (the integral of decelerating force with respect to deformation) before foam densification (at high strains) causes high deceleration (or force) [53]. Crash mats are used in a variety of conditions; protecting skiers, snowboarders and mountain bikers (who can travel at high speeds) from hazards on a mountain (i.e., lift poles or trees), often in extreme and variable climates, to providing padding to gymnasts on flat surfaces at room temperature.

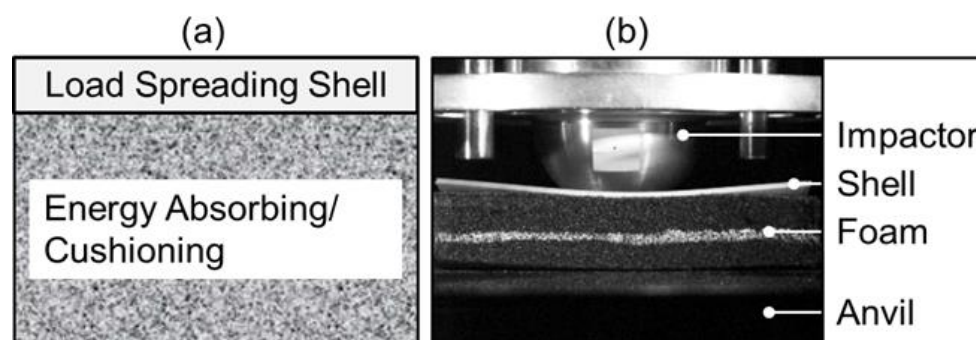


Figure 2. (a) Schematic of a typical piece of Personal Protective Equipment containing pressure dissipating material (hard outer shell) and energy absorbing/cushioning material (deformable foam); (b) Impact adapted from British Standard 6183-3:2000.

Sport safety equipment is often certified according to tests specified in standards and regulations (i.e., [54–58]), which typically specify a maximum allowable peak force/acceleration under impact (i.e., Figure 2b). To perform well in these tests, a product should absorb or dissipate as much energy as possible to prevent force/acceleration from passing its allowable limit [59]. Criteria within standards (such as impact energies, velocities and masses) are not always well justified and tests typically feature fixed rigid anvils rather than biofidelic (human like) surrogates, meaning they are not overly representative of the scenarios where the equipment may be required to perform [44]. In some cases there is no standard, so manufacturers certify products against a standard for another safety device, which can be misleading for consumers. McIntosh discusses the increased chance of injury when perceived protection offered by equipment is incorrect [19].

Crash mats are typically certified to BS EN 12503-1:2013 [60] as intended for gymnasium use, but include impact tests for outdoor activities such as pole vaulting. BS EN 12503-1:2013 is not reflective of the sometimes harsh and variable outdoor environment (weather conditions, surfaces, etc.) where these mats can be located, and tested parameters do not reflect realistic impacts [58]. There are

other occasions where specific standards are not available, and so a proxy is used. Two examples from snow sports are wrist protectors, certified to EN 14120:2003 [61] for roller sports [51], and back protectors, which are often certified to EN1621 (motorbike) [62]. Schmitt et al. found that snow sport participants expect back protectors to protect the spine, but EN1621 does not test against scenarios likely to cause spinal injury [18]. Inspection of PPE (impact shorts, knee guards, elbow guards and back protectors etc.) marketed for adventure sports including mountain biking, kayaking and snow sports shows EN1621 [62] & EN 14120:2003 [61] (for motor-biking) are repeatedly used in place of a dedicated standard.

Some standards have received criticism for not providing adequate tests even when applied to their intended field. Reaction to a number of high profile deaths and serious injuries as well as multiple awareness campaigns [63] raised the issue of helmet use in snow sports considerably, but head injury rates have remained fairly constant [63,64]. Scandals in the National Football League (NFL) culminated in high proportions of Chronic Traumatic Encephalopathy (CTE, up to 99% in a bias but large sample set) that could have contributed to early death, suicide and dementia in players [65].

In some cases, equipment and regulations intended to protect sports people are clearly unsatisfactory. As an example of equipment not meeting expectations, attenuation of rotational acceleration is thought to be critical in protection from concussion in sports [66,67]. Standards, however, typically assess helmets based upon their attenuation of linear accelerations (e.g., EN1077 & ASTM F2040, & F1446 [54,56,68]) and resistance to penetration (e.g., EN1077 [56]) based upon direct impacts [69,70]. Standards can be updated or replaced, for example BSI 6685-1985 for motorised vehicle helmets (a previous revision of Reference [71]) replaced BS2495:1977 and BS5361:1976 to include oblique impacts. The standard for cricket helmets (BS7928:1998) was amended (BS7928:2013) to include impacts by cricket balls [72] following findings that cricket helmets were not sufficiently attenuating acceleration under high speed impacts [73]. Commuter cycling (where cyclists travel alongside motor vehicles) is becoming increasingly popular due to clear benefits to health, congestion and emission levels, as well as improved facilities such as dedicated lanes. Safety concerns are a major barrier to participation in commuter cycling [74,75] but helmets are still only certified to protect from linear accelerations [76].

Sports equipment is a competitive, rapid uptake market. Manufacturers search for new technology to remain competitive, achieve the highest possible levels of certification and improve safety. One approach to solve the problem of rotational acceleration in helmets is a slip plane between the shell and crushable foam [77]. Slip plane technology is included in some commercial helmets, despite a lack of experimental evidence to support a reduction in concussion risk [78–81], highlighting the problem caused by insufficient standards. As an example of material development in sporting PPE, trends over the past twenty years have favoured lightweight, ergonomic equipment which does not sacrifice performance in standard tests [49]. Non-Newtonian fluids with high energy absorption were developed and can act as both a shell and cushion [82,83], offering comfort and flexibility under normal use and increased stiffness under impact. Non-Newtonian materials in isolation can pass certification tests for sporting PE and PPE [18,44,47,48,50]. Scientific literature highlights limitations in standards, as well as associated certified products including helmets [69,79–81], back protectors [18,50] and wrist protectors [51,84,85]. Recent trends look to include the use of more representative surrogates rather than rigid anvils [84,86,87] and tests designed for specific sports [50,51] to replace proxy standards (e.g., [61]). Solutions including novel materials are needed to reduce the effect of sports injuries and meet required improvements to standards (i.e., as per BSI 6685-1985 [71] and BS7928:2013 [72]).

3. Common Auxetic Materials and Structures

Auxetic research began in earnest with open cell foam [9], the first example of a man made NPR material. Subsequently, auxetic materials have now been developed or discovered in other nanocrystalline [88] and microporous [89] polymer, ceramic [90], metallic [91] and composite [92] forms, and include natural systems [93]. Auxetic materials such as foams, textiles and AM structures

are often classed as mechanical metamaterials; with unexpected macro-scalar (effective) characteristics caused by their micro/nano-structure [15].

This section will first discuss the modelling of auxetic structures and mechanisms, before considering auxetic foam fabrication, properties and characteristics, followed by some of the other auxetic materials of relevance including textiles and those manufactured by AM.

3.1. Modelling Auxetic Materials and Structures

Numerical [94–97], molecular [98] and FE models [99–101] have all been applied to auxetic materials. These models, used individually or combined, typically analyse the elastic deformation mechanisms of auxetic materials. The most common microstructures of cellular auxetics can be designated into three types; re-entrant, chiral and rotating units (Figure 3a–c). The 2D re-entrant structure (such as Figure 3a,d) was the first to be modelled numerically [95] and was developed in early work on auxetic honeycombs and foams. Other early models included a mechanical model of isotropic 2D/3D frameworks of rods connected by sliding collars [102] and a thermodynamic model of a 2D assembly of hard cyclic hexamer ‘molecules’ [103]. Chiral auxetics (Figure 3b)—asymmetric structures that are non-superimposable on their mirror image [104]—achieve NPR through cooperative node rotation-induced bending of connecting ligaments. Rigid rotating units (Figure 3c) can have NPR, dependent on the rotation of connected squares [105] or other shapes [106–108], and this model has been used as an alternative to the re-entrant model in auxetic foams [109]. Other models and structures exist, including the missing rib model [110], cellular systems featuring pre-defined mechanical instabilities [111] and the nodule-fibril model for polymers [112]. Auxetic behaviour induced by elastic instability includes systems consisting of 2D tessellation of elliptical [113] and other shape [114,115] voids and 3D tessellations of holes [116]. Non-porous sheets with tessellations of spherical dimples have also been investigated for auxetic response [117].

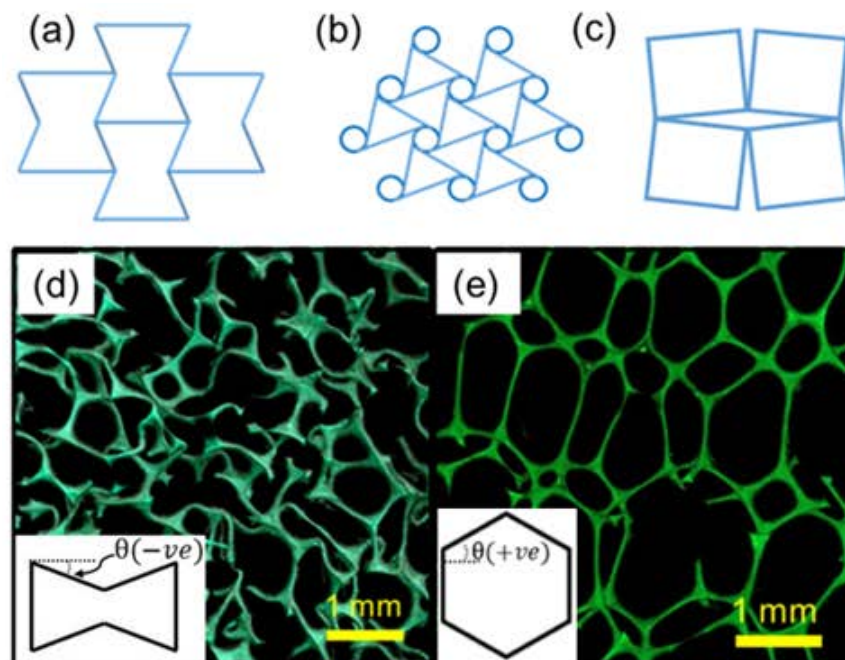


Figure 3. (a) Assembled 2D re-entrant structure; (b) 2D Chiral structure; (c) 2D rotating squares structure; (d) Micro Computed Tomography of polyurethane auxetic open cell foam (depth = 1 mm), pop-out showing simplified 2D diagram of a re-entrant cell, θ = re-entrant angle (negative value for angle below horizontal axes); (e) Micro CT scan of conventional open cell PU foam (depth = 1 mm), with pop-out showing simplified 2D diagram of a conventional polyhedral cell, θ = cell rib angle (positive value for angle above horizontal axes).

Re-entrant models have been used to investigate the deformation mechanics of cellular auxetics. Deformation due to flexure of the cell wall alone was initially considered, with the cell ribs assumed to behave as beams of uniform thickness [118]. Combined hinging (change of angle between ribs) and stretching (increase in rib length) of the cell wall was later modelled [98], as well as a 14-sided polyhedron, specifically for open cell foam, with cell rib bending as the main deformation mechanism [119]. All three deformation modes have been modelled simultaneously [96,120], confirming that the change of cell parameters (e.g., cell length or rib angle) directly affected Poisson's ratio and Young's modulus. The combined hinging, stretching and bending model [96] has been adapted to accurately predict the mechanical properties of gradient, isotropic and anisotropic auxetic foam [23].

Auxetic application in other fields has progressed with the use of FEM, such as auxetic cores used in sandwich plates that reduce shear stresses [121], anti-tetrachiral stents demonstrating desired radial expansion with axial stability [122] and smart auxetic honeycombs in structural health monitoring [123]. FEM can predict the effect of changing design parameters of auxetic structures, such as cell wall thickness [97,124], unit cell cross-sectional area [94], relative stiffness of modelled beams [125] and ratio of vertical to oblique cell wall length [126]. Simulation results could therefore aid and inform the design of future prototypes—e.g., to reduce a structure's mass while maintaining the maximum load it can support. FEM has also been used to develop understanding of the effect of plastic deformation on auxetic behaviour [127,128] and generate specific material models to explore impact resistance of auxetic honeycomb structures [129]. A framework for modelling auxetic foam using the continuum approach at large strains has been developed with FEM [130–132] and could be extended to model composite structures made from auxetic materials.

Several FEM studies established that the angle of re-entrant cell ribs effects Poisson's ratio [26,133–135], demonstrating cell parameter manipulation. FEM has also highlighted that other internal cell parameters (e.g., length, height, thickness) can be changed to tune the Poisson's ratio, and that flaws in the re-entrant cell structure can reduce NPR's magnitude towards zero [136]. Innovations are facilitated by FEM, such as the combination of two auxetic structures within one design (re-entrant hexagon and arrowhead) [137], honeycombs with ribs made of 2-phase composite material [138], the development of curved honeycomb unit cell designs [139], the creation of auxetic honeycombs inspired by the spider's web [140] and the formation of auxetic systems made out of readily available materials [141] and recycled rubber [142].

FEM has also been employed to model auxetic two-phase systems without voids by filling the spaces of a cellular first phase with a matrix second phase. This was an idea first postulated in 1992 and modelled analytically for elastically isotropic laminates by Milton [143] and using FEM for 'network embedded composites' by Evans and co-workers [144]. More recently, FEM has been extended to a two-phase core employing conventional and/or auxetic phases for out-of-plane auxetic behaviour [141], and to sandwich panel composites with the two-phase core employing established auxetic cellular structures and/or auxetic matrix [145–147], as well as structures developed using topology optimisation routines [145,148]. The ability to have temperature-dependent auxetic behaviour in such systems has also been investigated using FEM by allowing one or both phases to possess temperature varying Young's modulus [149,150].

The effect of design changes on Young's modulus and Poisson's ratio can be adjusted and improved before manufacture [121], and FEM can validate analytical results [151–158]. Full validation of FEM often requires comparison and agreement with experimental testing [159–167], which can potentially lead to extrapolation or tailoring of models for specific applications. Experimental test data can be input into FEM solvers to validate and develop material models [168]. With a validated model, design changes can be implemented and investigated without numerous iterations of manufacturing and testing. FEM can then be used alongside optimisation tools to further improve auxetic designs [169–173], although the 'modelling theory' remains to be examined stringently [174].

Dynamic effects can also be examined with explicit FEM solvers. The energy absorption of a re-entrant structure when crushed by a rigid wall has been analysed [175], but not experimentally validated. Analytical formulae were however used to validate FEM suggestions that auxetic honeycombs have higher energy absorption than conventional honeycombs in crushing strength analysis [176]. When varying the impact energy on a jounce bumper [27,177], FEM closely matched experimental values for the material's Poisson's ratio and compressive modulus and the jounce bumper's force and displacement. A subsequent auxetic bumper model showed less vibration in compression than a non-auxetic equivalent. A range of (FEM) parametric studies compared rate-dependent blast resistance performance in military applications [178,179]. Auxetic sandwich panels had higher impact resistance than their conventional counterparts, validated with comparison to analytical models rather than experimental data. Sporting PE and PPE typically aims to minimise harmful impact forces/accelerations through high strain rate compression of energy absorbing materials [180,181], and explicit solvers have previously facilitated such investigation [47,48,182].

3.2. Fabricating and Characterising Auxetic Foam

Auxetic foam is often fabricated to experimentally show expected enhancements (i.e., to impact force attenuation or vibration damping) due to NPR [2,3,33,183]. Auxetic foam fabrications typically change the cell structure of open cell foam (referred to herein as the parent foam) to give it an NPR. Lakes' thermo-mechanical fabrication method [9] first applies a volumetric compression ratio (VCR, normally defined as original/final volume and typically between 2 and 5 [184]) to a parent foam in all three orthogonal axes to buckle cell ribs [118]. The applied compression changes the cell shape and causes the re-entrant structure, as cell ribs buckle beyond ~5% compression [118]. The compressed foam is then heated to a set temperature to encourage permanent plastic deformation. The temperature is typically between 130 and 220 °C [13], often referred to as the 'softening temperature' [20,185]. Finally, the foam is cooled to fix the imposed structure [9]. Buckling the originally straight ribs (Figure 3e) gives the polyhedral cells a re-entrant, contorted cell structure [9] (Figure 3a,d). Typical sizes were initially small, in the order of 20 × 20 × 60 mm (following fabrication), although larger 'scaled up' samples have subsequently been fabricated (e.g., [185–188]).

Fabrication methods for auxetic foams have developed and diversified since Lakes' initial study [9]. Stretching samples after cooling was introduced to reduce adhesion between cell ribs and residual stresses [189]. More recently, fabrication processes have been split into stages including; multiple heating cycles (with foam removed from the mould and stretched by hand in between to reduce residual stresses, flaws and creases [190]) and the addition of an annealing stage—heating below the softening temperature. Foams are typically annealed at 100 °C [37,185,190], but alternatives to annealing include slow cooling in the mould in air [20,191] or cooling outside the mould in air [192]. In an attempt to reduce creases and flaws when inserting foam into the mould, olive or vegetable oil and WD-40 have been used to lubricate moulds [185,189,193].

Another line of investigation has attempted to increase the range of Poisson's ratios and Young's moduli achievable following thermo-mechanical fabrications. The heat, time and compression applied during fabrication can be adjusted to give higher magnitude NPR and increased stiffness [129]. Heating for longer or at a higher temperature ('over-heating' while using typical compression levels) gives a positive or near zero Poisson's ratio re-entrant foam [30,194]. Over-heated re-entrant samples have comparable density to typical auxetic foams and a linear stress strain curve without the presence of a plateau region [30,194]. Comparing auxetic and over-heated foam with a positive Poisson's ratio [194] could demonstrate the effect of Poisson's ratio on characteristics such as vibration damping or impact force attenuation.

In depth analysis shows the complexity and diversity of chemical constitution in polymers (including those found in foams) [20]. Polymeric microstructure [20], and microstructural changes caused by heating [195] have only recently been investigated in relation to auxetic foam fabrication. Li & Zeng targeted styrene acrylonitrile copolymer (SAN) particle bonding, which has a glass transition

temperature of around 110 °C. Such, or other, electron donating groups [15] can provide fixing mechanisms for imposed structures.

Sporting products often include foam sections which have a larger planar area than typical auxetic foam samples ($\sim 20 \times 20 \times 60$ mm) [9,185,196], and numerous scaled up fabrications have been attempted [4,7,23,185–187]. Large fabricated samples often exhibit random and ordered inhomogeneity. Random inhomogeneity is caused by flaws such as surface creasing [185], due to difficulty compressing large samples of foam into the mould [186]. Ordered inhomogeneity was observed in fabricated cubes (150 mm sides), where the centre had the lowest density [4,8]. Possible explanations include reduced compression towards the centre of the cube during fabrication or a thermal gradient that meant the internal structure was not sufficiently fixed and re-expanded following fabrication. The specific influence of temperature gradients and compression gradients during auxetic foam fabrication is unclear.

Solutions to increase homogeneity when fabricating large samples of foam include; (i) a mould with moveable walls which can be assembled around the foam and then used to apply compression [186,197]; (ii) a multi-stage compression process with an intermediate VCR to reduce insertion forces [185] and (iii) a vacuum bag to apply compression [187]. Vacuum bags can apply consistent pressure through thickness, reducing external densification and allowing fabrication of additional shapes (i.e., curved) [187]. Recent work utilising rods passing through large sheets of foam [7,8,23,188] is the only published method which seeks to apply controlled distribution of material within the mould. ‘Felted foams’ are fabricated commercially by compressing open cell foam between two heated plates to impart an anisotropic, re-entrant cell structure and direction dependent NPR [33].

Small scale fabrication parameters depend on the type of foam used and the compression levels applied [20,185]. It is likely that changes to fabrication parameters may be needed when ‘scaling up’ fabrications, and there may not be a ‘one size fits all’ style best approach. A comparative evaluation of gradual compression, vacuum bag compression and controlling internal compression using rods would, nonetheless, highlight advantages and disadvantages and aid selection and adaptation of the most appropriate method for fabricating large samples of auxetic foam.

Alternatives to the thermo-mechanical fabrication process [9] include using a solvent or softening agent instead of heating. Acetone [196] and pressurised CO₂ [21] can be used, depending on polymeric constitution and types of bonding present within the original foam. Softening methods can be combined, and both acetone [2] and CO₂ [21] have been used in combination with heat. Chemicals can be used to target specific bonds (i.e., SAN particle bonds) [20]. Liquid solvents (such as acetone) will require a drying phase and so some form of gradient is likely in larger samples. Provided there is no significant gradient due to diffusion of gases from the centre of samples during/after fabrication, the CO₂ softening route could reduce the effect of temperature gradients in thermo-mechanical fabrications.

Attempts to apply thermo-mechanical fabrication methods typically used for open cell foam to closed cell foam can rupture the foam’s cell walls [185,198]. NPR has still been achieved along one axis in closed cell low density polyethylene (LDPE) foam, by combining thermal softening (at 110 °C) and high hydrostatic pressure (662 kPa, applied by a pressure vessel) over 10 h and maintaining the pressure for a further 6 h after cooling [199]. Heating for an hour at 86 °C, then subjecting to vacuum pressure for 5 min prior to sudden restoration of atmospheric pressure also produced uniaxial NPR in the same LDPE closed cell foam [199]. Slow diffusion of gas through cell walls was similar to predicted values, suggesting the cell walls in the auxetic LDPE foam had remained intact. Solid state foaming (sticking together pieces of closed cell foam cut in a re-entrant shape) [200], syntactic foam processes (embedding degradable/collapsible beads with a re-entrant shape into a molten/liquid polymer) [201] and AM [202] have also produced auxetic foam-like structures.

Measuring strain in compliant, often inhomogeneous foam or foam like structures requires non-contact methods. Wide ranging studies, employing a variety of test protocols, have been undertaken to characterise auxetic polymeric foams for structural, mechanical, thermal, filtration

and impact properties, for example. Isotropic auxetic foams with Poisson's ratio between 0 and -0.7 have been reported (e.g., [3,9,20,22,23,189,195,203]). Higher magnitudes of NPR (<-1) have also been reported for anisotropic auxetic foams [187,190]. Density measurements of whole or dissected samples are useful in assessing the extent of, and variation in, volumetric compression throughout thermo-mechanically fabricated re-entrant foam [22,204]. Standardisation while characterising samples would help assess levels of agreement between different studies. Where possible future testing should be undertaken in accordance with, or based upon, the appropriate ASTM standard (e.g., ASTM-D412—15a [205]) for quasi-static tensile testing, which requires communication of sample dimensions, strain rate, range and measurement method and joining/contact methods between sample and test rigs.

3.3. Fabricating Auxetic Textiles

Auxetic textiles have the potential to contribute enhanced mechanical properties to textile applications in sport—including for apparel, equipment and injury prevention and treatment. Developments of auxetic fibres and fabrics, and their production methods, have enhanced the potential to use auxetic textiles commercially. Auxetic yarn with a high magnitude of NPR (<-2) can be produced from standard, non-auxetic fibre materials and conventional textile manufacturing processes [206]. Fabrics can, therefore, be manufactured from auxetic yarns without the need to develop new techniques.

The auxetic yarn in Reference [206] comprises a relatively high modulus thin wrap fibre around a lower modulus thick core. Both wrap and core components are typically conventional fibres. When extended the (initially helical) wrap fibre becomes straight and pushes the (initially straight) core fibre into a helix. Since the core is thicker than the wrap, the final stretched yarn is thicker with the helix core than the initial un-stretched yarn with a helical wrap. Due to the double helix nature of the wrap and core construction, the auxetic yarn is referred to in the literature as the double helix yarn (DHY) [207] and also the helical auxetic yarn (HAY) [208–211]. In this review we refer to this yarn as the DHY. Development of the DHY includes an auxetic plied yarn [212], auxetic braided structure [160], and a DHY where the 'wrap' fibre is stitched in place to offer more control over its behaviour by preventing fibre slippage [213]. Heat treatment has also been utilised to solve the issue of slippage [214]. The initial angle at which the wrap fibre is spun around the core fibre, and the diameter ratio of wrap to core fibre influences the value of the NPR, whereby a lower yarn wrap angle increases the magnitude of NPR [215–217]. The DHY offers increased energy absorption under impact [209].

The production of auxetic polymeric monofilament fibres has also been reported and utilises a process of continuous melt extrusion [218,219] to form a microstructure of interconnected surface-melted powder particles. NPR arises at the microscale of these monofilaments, in contrast to conventional filaments, for which mechanical properties, including Poisson's ratio, arise at the molecular (polymer chain) level [220]. The developed auxetic monofilaments have been used to demonstrate enhanced fibre pull-out resistance of auxetic fibres, requiring double the extraction force (than their conventional counterparts) [221], which could enhance the longevity and robustness of sports apparel and equipment.

Auxetic yarns and fibres have been incorporated into fabrics. The DHY has been employed to produce auxetic woven fabrics for composite reinforcement [206] and potentially as medical bandages [217]. Auxetic plied yarns have also been used in woven fabrics where yarns with shorter floating threads promote a greater magnitude of NPR in the fabric [222]. The auxetic monofilament has been used to develop knitted, woven and non-woven fabrics [223].

Auxetic fabrics can also be produced from conventional fibres. Out-of-plane NPR has been induced in non-woven fabrics, produced thermo-mechanically [224,225], via compression between two flat, heated plates to tilt and buckle needle punched fibre bundles. The through-the-thickness auxetic samples consist of bent fibre bundles perpendicular to the surface of the fabric. Under tension, the bent fibre bundle becomes re-orientated, in turn pushing on surrounding fibres and causing the fabric

thickness to increase. More recently, auxetic foldable woven fabrics have been fabricated through the use of conventional yarns and weaving technologies [226].

Knitting technologies offer the benefit of a high structure variety [29], enabling the fabrication of a range of different geometrical auxetic textile patterns. Auxetic fabrics can be manufactured using conventional yarns on commercial warp knitting machinery, which can be produced at rates and quantities comparable to non-auxetic warp knits [227]. Hexagonal structures are used for NPR warp-knitted textiles, including a rotational hexagonal structure [228] and re-entrant hexagonal net structures [229]. These hexagonal meshes have since influenced the fabrication of in-plane auxetic spacer fabrics (Figure 4a) [230,231]. Auxetic spacers exhibit excellent shape fitting to complex curves [232], high energy absorption and indentation resistance, and these properties could be enhanced with a greater magnitude of NPR [233]. Yarn loading capacity in NPR spacers affects tensile energy absorption [234], and FEM has successfully predicted the tensile NPR of a warp-knit spacer fabric [166]. Further research and tailoring of NPR spacers could aid the fit of sporting PPE that covers dome-like surfaces, such as protective head-wear [232].

Auxetic weft-knitted fabrics have also been fabricated with computerised flat knitting machines, based on three geometrical structures; (i) foldable structures (Figure 4b); (ii) rotating rectangles and (iii) re-entrant hexagons [235]. When using conventional yarns, the fibre type and geometrical structure are critical to the NPR of these fabrics and they can be adapted to tailor their Poisson's ratio and elastic modulus. Large NPRs (<-1) are possible, depending on the structure and yarns employed [235]. Auxetic foldable weft-knitted textiles have also been used as the reinforcement in polymeric composite materials [236]. Developments of auxetic weft-knitted fabrics will find a wide variety of potential applications in different fields, such as PPE for sportswear and headwear, but more research needs to be undertaken to explore these potential applications further [29].

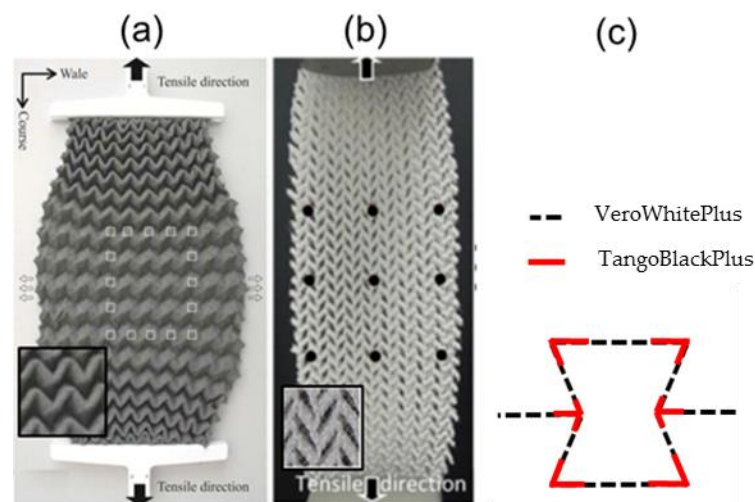


Figure 4. (a) Points marked on auxetic warp-knit fabric under tension [36]; (b) NPR effect of a weft knit fabric subject to extension [29]; (c) Dual-material auxetic metamaterial.

3D auxetic textiles have been developed for composite reinforcement applications [5,237]) through the use of warp and weft yarns [238] with stitch yarns [239] and auxetic fibres [240]. A four layer woven 3D auxetic textile structure has been used as composite reinforcement through a vacuum-assisted resin transfer moulding process [241]. Charpy impact tests (ASTM D6110-17 [242]) found the energy absorption of the auxetic textile was 6.7% higher than that of its conventional counterpart [241]. 3D Auxetic textiles have also been employed to reinforce a foam matrix fabricated by injecting and foaming [243,244]. With through-thickness NPR, 3D textiles may soon provide the enhanced protection associated with NPR materials to sports apparel and PPE [5].

There has, then, been a significant increase in the development and variety of auxetic fabrics since 2011. Due to the range of auxetic textiles under development and their unusual properties, these materials have a wide variety of potential applications [14]. For sports apparel, auxetic textiles could enhance comfort and performance in PPE, with the unique ability to fit easily to curved shapes combined with high compressive energy absorption and indentation resistance [245]. In order to implement auxetic textiles commercially, a future focus should be given to factors affecting their usage and wearability [246]. To embed or incorporate auxetic materials into sports garments, they should be relatively soft and flexible, lightweight, breathable and mouldable or available in a variety of shapes and thicknesses (5 to 10 mm). They may also be required to be homogeneous and/or joinable using flat lock seams [83].

3.4. Additively Manufactured Auxetic Materials and Structures

As alternatives to often inhomogeneous foams or textiles, the creation of auxetic materials with repeatable structures using various AM techniques has been investigated (e.g., fused deposition modelling [137], selective electron beam melting [175], selective laser sintering [247] and lithography-based ceramic manufacturing [248]). AM is a natural extension of FEM, as the existing modelling file can be converted to be compatible with most AM technologies to fabricate the modelled structure [167,249–252]. The AM structure can be experimentally tested to validate and potentially improve FEM [162,253–255], and key parameters can consequently be tuned and investigated with a particular application in mind.

Example materials used for AM in auxetic research include compliant rubbers and plastics. Metals and ceramics can also be made via AM but these studies have been omitted due to their incompatibility with sporting PE and PPE. Auxetic 3D chiral lattices have been modelled and produced by AM using TangoBlack® (Stratasys, Eden Prairie, MN, USA), a rubber-like AM filament [256]. AM has also combined two materials of different stiffness within; (i) one re-entrant unit cell [202,257,258] (Figure 4c); and (ii) novel chiral auxetic structures consisting of four ‘base’ unit cells surrounding a smaller ‘core’ chiral unit cell [259]. Using two materials of different stiffness provides a designer with greater control over unit cell deformation. The chiral auxetic has since been developed to use a re-entrant cell as the ‘core’ unit cell [260], meaning softer hinges are not necessary and the structure can be made from one filament material. The location and amount of each dual material provides additional ways to tune the mechanical properties (e.g., stiffness) of a structure without changing its geometry; as illustrated with the FEM of layered auxetic plates [261]. FEM and AM used in conjunction could facilitate such a parametric study with relative ease, for example by varying repeated structures [262].

AM structure’s Poisson’s ratio can be tuned by altering the geometry of a unit cell [263–265], enabling the design and analysis of novel auxetic structures using FEM [266,267] to help validate existing analytical formulae. Matlab has also been used to run FEM parametric analysis [167]. NinjaFlex®, (Ninjatek, Manheim, PA, USA) an elastic and flexible thermoplastic PU, has been used in the AM of auxetics [137,268–270], and in impact testing studies [269,270], with FEM used to highlight auxetic structures’ desired shock absorption capacity. Elsewhere, impact testing on non-auxetic NinjaFlex® honeycombs demonstrated that increasing strain rates (0.01 to 0.1 s^{-1}) resulted in an increase of energy absorbed (0.01 – 0.34 J/cm^3) [271]. Both strain rate and energy absorption are key considerations for auxetic material applications in sporting PE and PPE.

3.5. Gradient Materials

Gradient materials can be made from one material by varying its macro-structure to have different mechanical and structural properties in different regions (e.g., auxetic and conventional regions). Gradients can be discrete [22,23,272] or continuous [22,272]. Composite sandwich structures employing discretely gradient honeycombs have a higher compressive modulus and are stronger than conventional sandwich structures [41]. The same sandwich structures exhibit a large increase in bending stiffness at the transition between conventional and NPR regions [42]. Opposing synclastic/anticlastic (domed/saddled)

curvature associated with negative/positive Poisson's ratio respectively [9] cause increased shear modulus between regions and a localised stiffening effect. A similar stiffening effect can be seen in AM honeycombs with re-entrant inclusions during tensile tests [273]. Stiffening between discrete gradients of conventional and NPR could increase the bending stiffness (of the whole structure or specific regions) in sports equipment that contains honeycomb or fibre reinforced composites (e.g., skis, snowboards, tennis rackets and hockey sticks to name a few). Auxetic composite sandwich structures have not been tested for sports applications.

Gradient foams have been fabricated, by applying variable compression gradients to different sample sizes ($\sim 2 \times 2 \times 2$ cm to $\sim 30 \times 30 \times 2$ cm) using rods [22,23] and/or selecting mismatched uncompressed foam and mould shapes [22,23,272] (e.g., uniform foam sample compressed in a tapered mould). These gradient auxetic foam samples can exhibit vastly different cell structure and mechanical properties in different regions, which can be explained using an analytical model [23]. Gradient structures could be employed to foams or other materials (i.e., fabrics) to allow the development of garments which will fit to the wearer and adapt to their shape as they move.

4. Expected Characteristics and Supporting Evidence

Beneficial characteristics of auxetic materials include increased shear modulus, indentation resistance [10,30], dynamic [274,275] and static compressive energy absorption [8,37] and decreased bulk modulus [10,30]. Increased indentation resistance [30] and compressive energy absorption [2,8,33,37,204] have been shown experimentally in comparisons of auxetic and conventional foams. Lateral expansion due to axial tensile loading makes auxetic structures/materials ideal candidates for straps in apparel, increasing area to spread increasing loads and prevent 'digging in' [276]. Many of the characteristics which provide unique enhancements for auxetic materials come from Elasticity theory [10,277].

For isotropic materials experiencing elastic deformation, Young's modulus (E) and shear modulus (G) are related (Figure 5a, Equation (1)), as are Young's modulus and bulk modulus (K , Figure 5b, Equation (2)) [278]:

$$G = \frac{E}{2(1 + \nu)} \quad (1)$$

$$K = \frac{E}{3(1 - 2\nu)} \quad (2)$$

Elasticity theory states that Poisson's ratio must be between -1 and 0.5 for 3D isotropic materials [118,279,280], and between -1 and $+1$ for 2D isotropic materials [281]. From Equations (1) and (2), as Poisson's ratio tends towards -1 both shear (Equation (1)) and bulk (Equation (2)) modulus are driven towards extremely high or low values (respectively) in a 3D isotropic material.

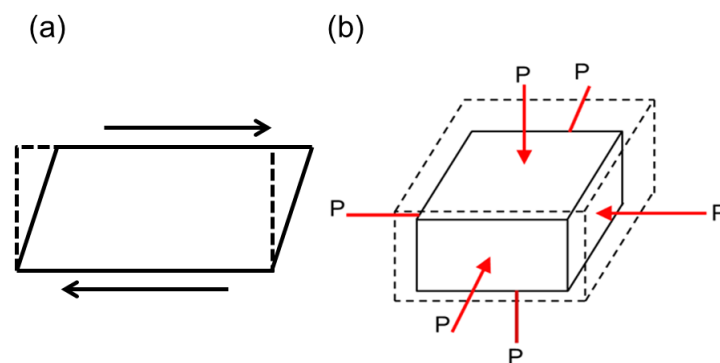


Figure 5. Schematic showing (a) shear deformation and (b) bulk/volumetric deformation. Black arrows show shear loading, red arrows show loading due to hydrostatic pressure, dashed lines show original (a) shape and (b) volume.

Indentation resistance is a measure of the load required to indent a material (Figure 6a,b). From elasticity theory, Hertzian indentation resistance (H , Equation (3)) for an isotropic material compressed with a uniform indenter depends on Poisson's ratio, Young's modulus and a constant (x) related to the shape of the indenter [31].

$$H \propto \left(\frac{E}{(1 - \nu^2)} \right)^x \quad (3)$$

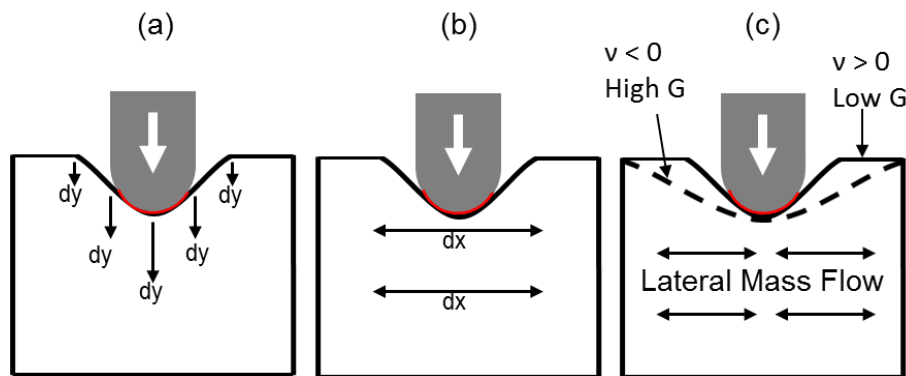


Figure 6. Simplified 2D indentation showing (a) Axial deformation; (b) Lateral deformation described in Equation (3); (c) Effect of large shear modulus (Equation (1)) on indentation area (---) and lateral mass flow, both un-accounted for in Equation (3). The red line shows contact area (Equation (4)).

A material with large indentation resistance, but low Young's modulus, could be used in a protective pad that will deform by a similar amount for high or low area (i.e., flat surface vs. studded) impacts. Such a pad would be more versatile, reacting to different surfaces to optimise its resistance to deformation [282]. Assuming a constant Young's modulus, as Poisson's ratio tends towards -1 , a material should exhibit infinitely higher resistance to shear deformation (Figure 5a, Equation (1)) and high indentation resistance (Figure 6, Equation (3)), while becoming increasingly easier to deform volumetrically (Figure 5b, Equation (2)). Infinite shear modulus and maximum indentation resistance and volumetric compressibility can only be achieved elastically and isotropically with auxetic materials [10], and increased indentation resistance has been shown experimentally [30,31,283].

Equation (3) for Hertzian indentation resistance comes from elastic properties and assumes; (i) the surfaces are continuous and have non-conforming profiles; (ii) the area of contact (Figure 6) is much smaller than the characteristic dimensions of the contacting bodies; (iii) the strains are small and purely elastic and (iv) the surfaces are frictionless at the contact interface. These four assumptions for Hertzian indentation are not always held, although Equation (3) is often referred to and discussed in the context of non-Hertzian indentations [284,285]. Sporting PPE typically has a low thickness, so does not often meet assumption (ii). A finite thickness model has been developed for soft and thin cushion materials where Hertzian theory is expected to become invalid, and auxetic cushions were found to reduce the contact pressure on the buttocks (indenter) [286]. In another approach, Equation (3) has been adapted for thin sheets of rubber [287], to include a correctional multiplier based on a ratio of contact area between the sheet and indenter (A_t , Figure 6) and the sheet's thickness (a_t) (Equation (4)). As thickness decreases towards zero, contact area/thickness increases and the correction tends towards unity. The force required to indent rubber to a specific depth increases as thickness decreases, but it is unclear if the same trend applies to NPR materials. The final assumption of zero friction has been shown through FEM and continuum mechanics to be invalid in simulations of infield situations [285,288–290]. In these simulations, friction was found to enhance NPR's contribution to indentation resistance.

$$Correction = 1 - \exp^{-\frac{A_t}{a_t}} \quad (4)$$

Equations (3) and (4) are for instantaneous, linear values. They do not, therefore, account for the different amounts of densification and possible hardening caused by lateral deformation due to Poisson's ratio (Figure 6c). Auxetic foam (with a relatively high shear modulus, Equation (1)) should resist shear deformation more than its conventional counterpart. Auxetic foam's upper surface would, therefore, compress as a larger, flatter area (represented by the dashed line, Figure 6c) as shown in cylindrical indentations [30] and using FEM [291]. FEM and analytical models also report a reduction in contact area for simulations with NPR materials [292], suggesting that deformation occurred over a larger radius, rather than the foam wrapping around the indenter. The opposite effect (auxetic foam wrapping around the indenter) has been predicted in FEM simulations of low strain indentation of 2D linear-elastic isotropic blocks [183] and also observed during impacts with a hemispherical dropper onto samples covered with 1 to 2 mm thick polypropylene sheets [3]. In the FEM study, a lower Young's modulus as well as NPR was employed for the auxetic foam, providing a shear modulus almost a factor of 2 lower than the conventional foam (Equation (1)), which possibly explains the discrepancy. In the experimental study, the added complexity when considering multi-material systems (e.g., featuring a stiff shell and compliant foam), hemispherical or studded indenters (rather than cylindrical) and high strain rates caused by impact could explain the observed differences. The relationship between the shell and foam's elastic moduli (as discussed in relation to coatings [293,294]), the foam's Poisson's ratio [292,294] and synclastic/anti-synclastic (domed or saddled) bending in the upper surface may affect indentation resistance.

Hertzian indentation requires corrections for high strain indentations, impacts of non-linear materials or multi-material systems typical in sporting PPE [47,48] and, therefore, testing of auxetic foams for sports applications [285,288]. As noted above, friction (assumption iv) is expected to amplify increases in indentation resistance caused by NPR [285,288], and a correction factor has been applied [288]. Experimental indentations of auxetic materials, particularly foams, are not common [7,30], although some limitations of Hertzian indentation theory have been noticed and discussed [30]. Further significant modelling and experimental research examining NPR's effect on indentation responses of conforming, non-linear, anisotropic materials subject to a range of indenter sizes and shapes is therefore required.

One of the difficulties in testing NPR's effect on expected benefits (i.e., impact force attenuation or indentation resistance) when using foam is changes to Young's modulus and stress-strain relationships following fabrication [9,295]. Studies report auxetic foams with lower initial Young's modulus than their conventional counterparts [189,274,295]. Reduced Young's modulus has been attributed to the presence of buckled ribs in the auxetic foam being easier to deform than the straighter ribs of the conventional foam [295]. Elasticity theory (Equation (1), Figure 5a) also supports a reduction in Young's modulus as Poisson's ratio decreases if shear modulus remains constant. Auxetic foams typically have a higher density than their open cell parent foam, so the reduction in Young's modulus is contrary to the usual expectation of an increase in Young's modulus with increased density [118]. Note, though, that Gibson and Ashby refer to a density increase caused by thicker ribs, whereas in the auxetic foam fabrications density increases due to changes in rib orientation. Gibson and Ashby's cellular solid theory actually indicates that Young's modulus can either increase or decrease when moving from a hexagonal to a re-entrant cell geometry, characteristic of auxetic foams [118]. The increased Young's modulus is allowed by elasticity theory—materials with the same bulk modulus (Equation (2), Figure 5b) will have increased Young's modulus as Poisson's ratio decreases. Increases [2,190,197,204] as well as the aforementioned decreases in Young's modulus [9,274,295] have been reported in auxetic foam fabrications.

The re-entrant structures in auxetic foams typically give an initially quasi-linear compressive stress-strain curve, with hardening as pores close at higher compression levels ($> \sim 50\%$) [9,183,185,275,282]. Conventional open cell foams exhibit a low-stiffness plateau region due to buckling of cell ribs between $\sim 5\%$ and 80% strain (Figure 7a) [118]. Both of these cases have been explained numerically and validated experimentally [23,118]. It should be noted that the relatively linear and plateauing

stress-strain relationships only apply to specific forms of cellular materials that adapt a re-entrant structure, including PU foams [9,23] and 2D honeycombs [96]. Exceptions have been recently presented; re-entrant auxetic PU foams with a plateau region [23,195].

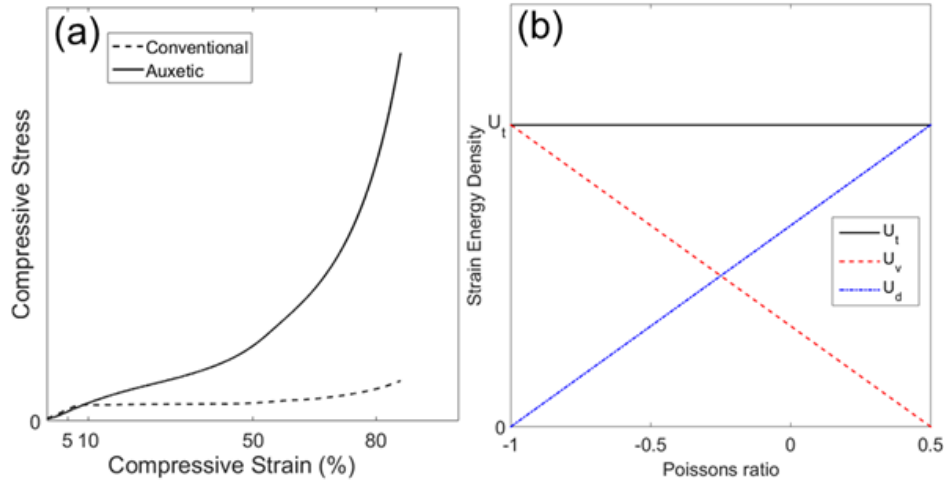


Figure 7. (a) Typical compressive stress vs. strain response of auxetic and conventional open cell foam (note cellular collapse between 5 to 10% then hardening beyond 80% strain via densification in open cell foam); (b) Strain energy density (Volumetric (U_v , Equation (5)), Distortion (U_d , Equation (6)) & U_t , Total) vs. Poisson's ratio for a linear elastic isotropic material subject to a uniaxial stress. Uniaxial stress and Young's modulus set to 1 kPa.

For a linear elastic isotropic material subject to a uniaxial stress (σ), the total strain energy density (U_t) is the sum of the volumetric strain energy density (U_v) and the distortional strain energy density (U_d), which are related to the Young's modulus and Poisson's ratio (i.e., [278]):

$$U_v = \frac{(1 - 2\nu)\sigma^2}{6E} \quad (5)$$

$$U_d = \frac{(1 + \nu)\sigma^2}{3E} \quad (6)$$

In Figure 7b, an applied compressive uniaxial stress and Young's modulus are arbitrarily equated to 1 kPa for simplicity. Plotting these values in Equations (5) and (6) between elastic limits of -1 and 0.5 for Poisson's ratio (Figure 7b) shows an increase in volumetric strain energy density and a reduction in distortional strain energy density as Poisson's ratio tends towards -1 . Auxetics material's tendency to volumetric (rather than distortional deformation) could effectively increase indentation resistance (Figure 6c, Equations (3) and (4)). As Poisson's ratio decreases, so does the stress concentration at a crack's tip, preventing crack propagation and increasing toughness [296,297]. Von Mises and maximum shear stress theory both define failure when distortional strain energy exceeds a maximum value. The reduction in distortional strain energy (to zero, Figure 7b) as Poisson's ratio reduces to -1 [279] is, then, expected to lead to an increase in toughness. A natural example of where this may be exploited may be found in the nacre layer of certain seashells. Nacre has a reported tensile NPR of the order of ~ -0.1 [93] and ~ -0.4 [298] which is thought to increase volumetric strain energy density by \sim eleven times while more than halving distortional strain energy density, allowing the system to absorb more energy before failure [298].

Increased energy absorption has been shown experimentally for auxetic foam; under flat plate [33] and studded impacts [274], quasi-statically with flat compression plates [8], within aluminium tubes [299] and with a studded indenter and a stiff shell [7]. When compressed cyclically at high strain rates (0.036 to 0.36 s^{-1} [300] and 0.033 s^{-1} [2,274]) auxetic foams absorbed up to sixteen times more

energy than open cell foams of a different polymeric composition and equivalent density, therefore appearing more useful in cushioning layers of sporting (and general) PE & PPE. The differences in energy absorption do not account for changes in stress/strain relationship or strain rate dependency between conventional and auxetic samples. As strain rates increased, Young's modulus and the magnitude of NPR increased marginally in samples of auxetic PU foam [301]. In some cases the increased linear elastic range of the auxetic foam compared to the parent foam with a plateau region in the stress-strain relationship could have contributed to higher energy absorption [2,8,33].

Energy absorption, strain rate dependency and (often) indentation resistance combine to influence performance under impact. Theoretically beneficial for impact protection [282], auxetic foam samples have been shown to exhibit between ~three and ~eight times lower peak force under 2 to 15 J impacts adapted from BS 6183-3:2000 for cricket thigh pads [3,8,55]. During a comparison of high strain rate compression (20 to 40 J) to a conventional commercial foam of similar density, auxetic samples exhibited (1.2 to 1.8 times) higher peak acceleration, but also exhibited higher compressive elastic modulus [2]. Peak forces can be further decreased (1.2 to 1.5 times) during 5 J impacts by impregnating auxetic foam with shear thickening fluid [302].

Inward material flow has been shown under impact by rudimentary visual inspection of high-speed camera stills, and the samples with the greatest magnitude of NPR exhibited higher lateral contraction, lower through thickness deformation and a similar peak force to other samples [33]. Newly developed 3D auxetic textile composites exhibit lower peak forces than their conventional counterpart under 12 to 25 J impacts [5]. In helical yarns, a wrap angle of 27° gave the best combination of Poisson's ratio and stiffness for energy absorption [209] during 7 to 65 J impacts.

Honeycomb sandwich panels with auxetic cores were found to resist ballistic impacts better than regular or rectangular cores [303], and absorb more impact energy when the re-entrant cell structure was non-uniform [304]. Laminated composites containing warp knit auxetic Kevlar® fabric reinforcement, under 167 m/s impact with a 14.9 g bullet (~200 J), showed similar energy absorption to laminates containing conventional woven Kevlar® reinforcement [305,306]. The auxetic Kevlar® laminates, however, displayed enhancements in fracture toughness (225%) and fracture initiation toughness (577%), and a reduction in front and rear face damage area [305,306]. Auxetic composite laminates displayed reduced back face damage during 7–18 J impacts by a stud [32,307,308]. Auxetic composite laminates could, therefore, improve the durability of protective shells in PPE and other sports equipment (i.e., bicycle frames or boat hulls).

Related to energy absorption, auxetic foams have been tested for vibration damping (to ISO 13753 for vibration protecting gloves [309]). At low frequencies (<10 Hz), auxetic foam exhibited lower transmissibility than iso-volume open cell samples made from the parent foam and iso-density uni-axially compressed samples [193]. Auxetic foam had a lower cut off frequency than its parent foam [310]. The transmissibility of auxetic samples was greater than 1 between 10 and 31.5 Hz, but less than 1 over 31.5 Hz [183], equivalent to commercial anti-vibration gloves. Auxetic foams also fatigued uniquely, with higher permanent compression than their parent foam and a general increase (as opposed to the conventional foam's decrease) in measured hardness after 80,000 cycles up to ~120 N (150 mm sided cubic samples) [311].

Curvature of a beam or plate subject to an out-of-plane moment is related to Poisson's ratio [9,312]. Sheets with a positive Poisson's ratio will adopt a saddled shape (anticlastic curvature, Figure 8a) and those with NPR will dome (synclastic curvature, Figure 8b). Doming is caused by axial (due to loading) and lateral (due to Poisson's ratio) extension on the upper surface combined with equivalent contractions on the lower surface. Conventional materials will contract laterally on the upper surface and expand laterally on the lower surface.

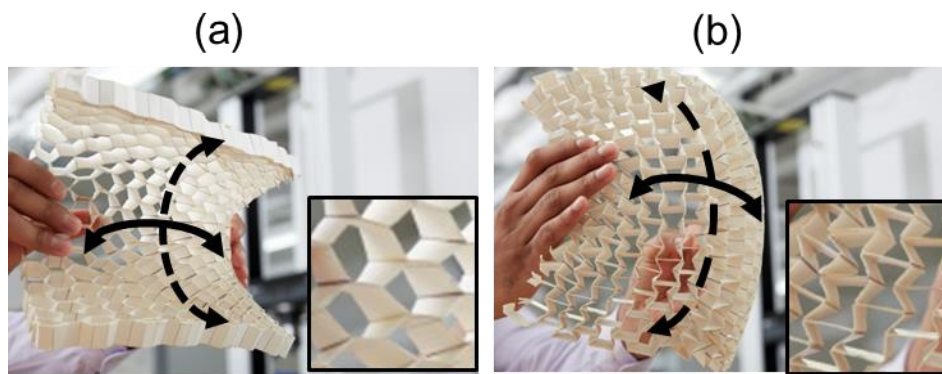


Figure 8. (a) Conventional honeycomb showing saddled curvature; (b) Re-entrant auxetic honeycomb showing domed curvature. Solid arrows show applied bending and dashed arrows show bending due to Poisson's ratio. Enlarged pop outs show cell structure.

Synclastic curvature has been observed in auxetic foam [9], analysed in detail in sandwich structures with an auxetic honeycomb core and auxetic laminate skins [312] and demonstrated by FEM [37,313] and experimentally using a simple paper model [37]. Auxetic fabric can conform around a spherical surface [36]. Deformation shape could be complicated to predict in nonlinear and often inhomogeneous auxetic foams [4]. Bespoke complex curvatures are achievable for gradient honeycombs displaying conventional and NPR regions when subject to an out-of-plane moment [314].

Some auxetic PU foam samples have been shown to exhibit shape memory, meaning they return to their original dimensions when heated [315] or exposed to solvents [196]. Shape memory auxetic foams investigated by heating in an oven returned rapidly towards their original dimensions when the temperature reached 90 °C. Samples had reached their original dimensions by the time the oven reached the original fabrication temperature of 135 °C.

Marginally re-entrant structures with NPR which exhibit partially blocked shape memory have been fabricated [195]. The fabrication process included numerous cycles of thermo-mechanical fabrication followed by reheating to return samples towards their original state. Auxetic behaviour was found in 'returned' samples from the third returned stage onwards, and has been attributed to the presence of kinked or corrugated ribs. Clearly shape memory could be detrimental in terms of sport safety equipment, as pads could be changed irreparably when exposed to heat or solvents (i.e., when machine washed or dried). Blocking shape memory [195] or investigating solutions to prevent a return to original dimensions (such as constraining auxetic foam in an outer textile/shell layer) could improve a product's lifecycle.

Several characteristics change in the auxetic foam fabrication process, including Poisson's ratio, stress/strain relationships and density [3,4,8,9,23,185,190,316]. So, during comparative impact tests between auxetic and parent foam [2–4,7,8,33,204,316], the specific contribution of individual characteristics, including Poisson's ratio, can be difficult to determine, and unambiguous experimental verification of theoretical enhancements due to the NPR requires further work. The same can be said for other studies into auxetic foam, including those into vibration damping [183,193], resilience/strength [317] and energy absorption [37].

Comparing results from scientific literature suggests that the compressive Young's modulus (30 to 50 kPa) of auxetic open-cell PU foams [3,4,118,185,316] is typically more than twenty times lower than that of the closed cell foams often found in sporting PPE (~1 MPa) [43,47–49,52]. Such a large reduction in stiffness suggests that the two materials are not comparable and stiffer auxetic foam is required for sporting PPE. The enhancements provided by NPR (e.g., indentation resistance) might allow for some reduction in stiffness, but to absorb an equivalent amount of energy to current sporting PPE, current auxetic foam would need a contribution from having NPR that would increase energy absorption by ~twenty times. The largest reported increase in energy absorption for auxetic vs. conventional foam

is sixteen times during dynamic cyclic tests [300], but increases of ~three times are more common in single impacts/compressions [8,33,204]. Crash mats are typically softer than PPE (~50 kPa [59]) and (due to their extensive variety of possible applications and impact scenarios) could benefit from the increased energy absorption and indentation resistance associated with auxetic foams [7]. The authors are not aware of any publications specifically comparing impacts or indentations of auxetic foam to foam typically found in sports PE and PPE.

5. The Potential for Auxetic Materials in Sports Products

The sporting goods sector is characterised by early uptake of new technologies and rapid product development, launch and replace cycles. Consequently, this sector is amongst the first to see commercial products based on auxetic materials, with two commercial sports shoe ranges that utilise auxetic structures. The Under Armour Architech sports shoe range [28] incorporates either an AM or moulded auxetic re-entrant latticed upper (Figure 3a) which is claimed to aid conformability around domed shapes, fit and comfort. The added manufacturing benefit of being formable as a one-piece upper, rather than several pieces each individually cut to shape and stitched together is also claimed. The Nike Free RN Flyknit sports shoe [34], on the other hand, employs an architected closed cell foam outsole with an auxetic rotating triangles structure (shown in Figure 9, first proposed in [105–107]). The outsole is claimed to exhibit bi-axial growth as the wearer accelerates or changes direction, for improved traction and impact energy absorption.

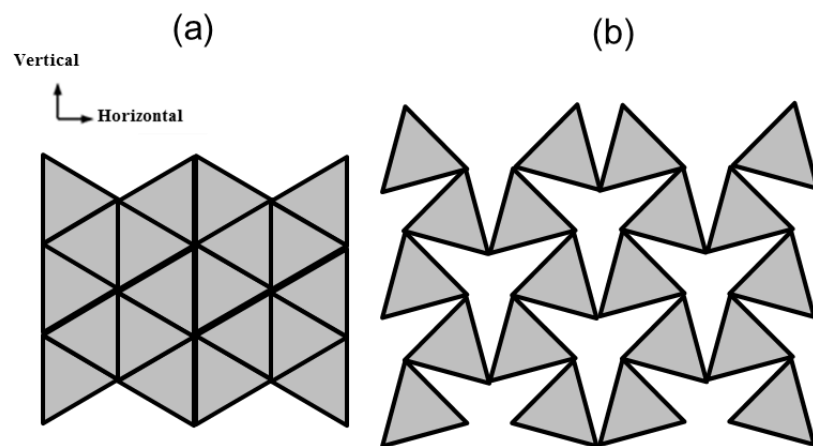


Figure 9. Schematic showing (a) rotating triangles (un-deformed); (b) rotating triangles' multi axial expansions (rotation = 15°), tensile load applied either vertically or horizontally.

Multi-axis expansion (due to NPR) has potential benefits in cleaning/shedding of dirt [39]. Multi-axis expansion could be implemented in a conformable facemask [35] to protect against extreme weather during outdoor/adventure sports, or commuter cycling—expanding bi-axially when the mouth is opened to increase breathability [9,38–40]. Other benefits of multi-axis expansion include large volume change, allowing design of small, easily stored garments which can expand when worn (i.e., for spare layers in outdoor/adventure sports).

D3O market the Trust Helmet Pad System [318] incorporating pads with a re-entrant auxetic geometry that are claimed to provide increased fit to the head and decreased acceleration under blunt impact. More products are likely to emerge if the increased level of comfort and protection offered by auxetic materials can be further demonstrated, justifying investment in the development of stiffer, more appropriate auxetic materials (such as closed cell [199] or shear thickening fluid impregnated [302] auxetic foams, or novel impact hardening auxetic polymers [319]). The emergence of sports products including auxetic materials could be assisted by the development of a commercially-viable (low cost, large scale) auxetic foam production process [23,185,186]. 'Felted' foams, fabricated by uniaxial

compression, are already commercially produced and exhibit auxetic behaviour in one loading direction [33]). Alternatively AM is a commercially viable option [28] to provide fine control over unit cell structure for auxetic foam-like structures.

The ability to change the shear modulus of a material through Poisson's ratio [118,151] could provide a useful tool in designing head protection that can reduce rotational acceleration [6]. When used in place of a comfort layer in a helmet, auxetic foam can significantly reduce the severity of direct impacts in comparison to its conventional counterpart [320]. Helmets and helmet certification standards have been criticised for focussing solely on direct rather than both direct and oblique impacts [69]. Controlling shear modulus by changing Poisson's ratio (to negative or positive values) of any layer within the helmet could contribute to solutions to reduce rotational acceleration (i.e., in combination with or instead of slip plane technology [77]). The benefit of using Poisson's ratio to change shear modulus is that elastic moduli would change less, limiting the effect on linear acceleration and therefore perceived performance according to current certification standards [66,67].

6. Conclusions

In a competitive, rapid uptake market such as sports equipment, it is important to keep searching for new and improved designs and materials. With frequent, catastrophic high-profile injuries and scandals (particularly involving head injury) the importance of improvement increases. The chance to increase market revenue, while reducing costs to health services, national economies and burdens on injured individuals, warrants continued research through commercial and state investment.

Auxetics have a wide range of potentially useful characteristics, including increased indentation resistance, vibration damping and shear modulus as well as decreased bulk modulus. These have been shown using auxetic foam compared to its parent foam and iso-density conventional foams. Further experimental comparisons of auxetic and conventional foam's indentation resistance, impact force attenuation and vibration damping are required to determine contributions from other variables, such as elastic modulus and density, to clearly identify the contribution due to Poisson's ratio.

The creation of auxetic foams appropriate and beneficial to sporting goods will require development of fabrication processes, especially for larger samples. Fabricating samples with comparative characteristics (e.g., Young's modulus and density) is also required to show the NPR's benefits (i.e., to indentation resistance). The solvent and CO₂ softening routes provide alternative and, in the latter case, faster auxetic foam fabrication. Increasing the stiffness of auxetic foam closer to the closed cell foam found in sporting PPE or ensuring that impact energy absorption is equivalent or higher is an important step for commercialisation. With dynamic energy absorption reported up to sixteen times greater in auxetic foams some reduction in stiffness is likely acceptable, but requires confirmation by appropriate testing. AM presents an alternative for the creation of auxetic cellular solids with bespoke properties. There is increasing confidence, then, that commercial auxetic foam production will be achievable, either by AM or by improved fabrication methods from open cell foams. Commercially available auxetic foam would improve access, allowing more sport safety equipment manufacturers to design, test and evaluate auxetic prototypes.

Another option to increase auxetic materials range of moduli and impact force attenuation is combining materials. Auxetic foam's impact force attenuation increased up to ~1.5 times when supported by shear thickening fluid. Enhancing the characteristics of auxetic fabrics and textiles by combining with a conventional, gradient or auxetic material could facilitate the production of sports garments and performance apparel that deforms with the wearer and attenuates impact forces. Combining conventional and auxetic sections of honeycombs in gradient sandwich structures increases bending stiffness close to transitions. Snowboards, skis, tennis rackets and hockey sticks (to name a few) use conventional sandwich structures, and could benefit from increased rigidity or equivalent rigidity and lower mass.

The more obvious characteristics of auxetic materials that are backed up with strong supporting evidence (multi axis expansion and domed curvature) have been implemented as auxetic foam and AM

materials into sporting footwear and helmet pad products. Commercial success for auxetic sporting PPE requires stronger supporting evidence that responds to trends accurately re-creating infield collisions and falls. Other auxetic materials such as laminates and knitted/woven fabrics that exhibit characteristics including increased fracture toughness and, potentially, tailorable shape change, are currently untested for sports applications within the peer-reviewed scientific literature. Unlike auxetic foam production, the fabrication of auxetic composite laminates and many of the auxetic fabrics is via established commercial processes, requiring little or no modification. With further development and testing auxetic laminates and fabrics could be applied to a range of sporting products, from carbon fibre reinforced composite bicycle frames to swim suits or rugby tops that deform with the movements of the wearer.

Conflicts of Interest: The authors declare no conflict of interest.

References

1. Evans, K.E. Auxetic polymers: A new range of materials. *Endeavour* **1991**, *15*, 170–174. [\[CrossRef\]](#)
2. Lisiecki, J.; Błazejewicz, T.; Kłysz, S.; Gmurczyk, G.; Reymer, P.; Mikułowski, G. Tests of polyurethane foams with negative Poisson's ratio. *Phys. Status Solidi Basic Res.* **2013**, *250*, 1988–1995. [\[CrossRef\]](#)
3. Allen, T.; Shepherd, J.; Hewage, T.A.M.; Senior, T.; Foster, L.; Alderson, A. Low-kinetic energy impact response of auxetic and conventional open-cell polyurethane foams. *Phys. Status Solidi Basic Res.* **2015**, *9*, 1631–1639. [\[CrossRef\]](#)
4. Duncan, O.; Foster, L.; Senior, T.; Alderson, A.; Allen, T. Quasi-static characterisation and impact testing of auxetic foam for sports safety applications. *Smart Mater. Struct.* **2016**, *25*, 54014. [\[CrossRef\]](#)
5. Zhou, L.; Zeng, J.; Jiang, L.; Hu, H. Low-velocity impact properties of 3D auxetic textile composite. *J. Mater. Sci.* **2017**, *53*, 3899–3914. [\[CrossRef\]](#)
6. Taha, Z.; Hassan, M.H.A. Parametric Analysis of the Influence of Elastomeric Foam on the Head Response during Soccer Heading Manoeuvre. *Procedia Eng.* **2016**, *147*, 139–144. [\[CrossRef\]](#)
7. Allen, T.; Duncan, O.; Foster, L.; Senior, T.; Zampieri, D.; Edeh, V.; Alderson, A. Auxetic foam for snowsport safety devices. In *Snow Sports Trauma and Safety, Proceedings of the International Society of Skiing Safety*; Springer: Cham, Switzerland, 2016; pp. 145–159.
8. Duncan, O.; Foster, L.; Senior, T.; Allen, T.; Alderson, A. A Comparison of Novel and Conventional Fabrication Methods for Auxetic Foams for Sports Safety Applications. *Procedia Eng.* **2016**, *147*, 384–389. [\[CrossRef\]](#)
9. Lakes, R.S. Foam Structures with a Negative Poisson's Ratio. *Science* **1987**, *235*, 1038–1041. [\[CrossRef\]](#) [\[PubMed\]](#)
10. Evans, K.E.; Alderson, A. Auxetic materials: Functional materials and structures from lateral thinking! *Adv. Mater.* **2000**, *12*, 617–628. [\[CrossRef\]](#)
11. Yang, W.; Li, Z.M.; Shi, W.; Xie, B.H.; Yang, M.B. On auxetic materials. *J. Mater. Sci.* **2004**, *39*, 3269–3279. [\[CrossRef\]](#)
12. Greaves, G.N.; Greer, A.L.; Lakes, R.S.; Rouxel, T. Poisson's ratio and modern materials. *Nat. Mater.* **2011**, *10*, 823–837. [\[CrossRef\]](#) [\[PubMed\]](#)
13. Critchley, R.; Corni, I.; Wharton, J.A.; Walsh, F.C.; Wood, R.J.K.; Stokes, K.R. A review of the manufacture, mechanical properties and potential applications of auxetic foams. *Phys. Status Solidi Basic Res.* **2013**, *250*, 1963–1982. [\[CrossRef\]](#)
14. Prawoto, Y. Seeing auxetic materials from the mechanics point of view: A structural review on the negative Poisson's ratio. *Comput. Mater. Sci.* **2012**, *58*, 140–153. [\[CrossRef\]](#)
15. Kolken, H.M.A.; Zadpoor, A.A. Auxetic mechanical metamaterials. *RSC Adv.* **2017**, *7*, 5111–5129. [\[CrossRef\]](#)
16. Lakes, R.S. Negative-Poisson's-Ratio Materials: Auxetic Solids. *Annu. Rev. Mater. Res.* **2017**, *47*, 63–81. [\[CrossRef\]](#)
17. Ren, X.; Das, R.; Tran, P.; Ngo, T.D.; Xie, Y.M. Auxetic metamaterials and structures: A review. *Smart Mater. Struct.* **2018**, *27*, 23001. [\[CrossRef\]](#)
18. Schmitt, K.U.; Liechti, B.; Michel, F.I.; Stämpfli, R.; Brühwiler, P.A. Are current back protectors suitable to prevent spinal injury in recreational snowboarders? *Br. J. Sports Med.* **2010**, *44*, 822–826. [\[CrossRef\]](#) [\[PubMed\]](#)

19. McIntosh, A.S. Biomechanical considerations in the design of equipment to prevent sports injury. *Proc. Inst. Mech. Eng. Part P* **2011**, *226*, 193–199. [[CrossRef](#)]
20. Li, Y.; Zeng, C. On the successful fabrication of auxetic polyurethane foams: Materials requirement, processing strategy and conversion mechanism. *Polymer* **2016**, *87*, 98–107. [[CrossRef](#)]
21. Li, Y.; Zeng, C. Room-Temperature, Near-Instantaneous Fabrication of Auxetic Materials with Constant Poisson's Ratio over Large Deformation. *Adv. Mater.* **2016**, *28*, 2822–2826. [[CrossRef](#)] [[PubMed](#)]
22. Sanami, M.; Alderson, A.; Alderson, K.L.; McDonald, S.A.; Mottershead, B.; Withers, P.J. The production and characterization of topologically and mechanically gradient open-cell thermoplastic foams. *Smart Mater. Struct.* **2014**, *23*, 55016. [[CrossRef](#)]
23. Duncan, O.; Allen, T.; Foster, L.; Senior, T.; Alderson, A. Fabrication, characterisation and modelling of uniform and gradient auxetic foam sheets. *Acta Mater.* **2017**, *126*, 426–437. [[CrossRef](#)]
24. Gatt, R.; Attard, D.; Farrugia, P.S.; Azzopardi, K.M.; Mizzi, L.; Brincat, J.P.; Grima, J.N. A realistic generic model for anti-tetrachiral systems. *Phys. Status Solidi Basic Res.* **2013**, *250*, 2012–2019. [[CrossRef](#)]
25. Yang, L.; Harrysson, O.; West, H.; Cormier, D. Modeling of uniaxial compression in a 3D periodic re-entrant lattice structure. *J. Mater. Sci.* **2013**, *48*, 1413–1422. [[CrossRef](#)]
26. Scarpa, F.; Panayiotou, P.; Tomlinson, G. Numerical and experimental uniaxial loading on in-plane auxetic honeycombs Numerical and experimental uniaxial loading on in-plane auxetic honeycombs. *J. Strain Anal. Eng. Des.* **2000**, *35*, 383–388. [[CrossRef](#)]
27. Wang, Y.; Ma, Z.D.; Wang, L. A finite element stratification method for a polyurethane jounce bumper. *Proc. Inst. Mech. Eng. Part D J. Automob. Eng.* **2016**, *230*, 983–992. [[CrossRef](#)]
28. Toronjo, A. Articles of Apparel Including Auxetic Materials. U.S. Patent 20140059734 A1, 6 March 2014.
29. Liu, Y.; Hu, H.; Lam, J.K.C.; Liu, S. Negative Poisson's Ratio Weft-knitted Fabrics. *Text. Res. J.* **2010**, *80*, 856–863.
30. Chan, N.; Evans, K.E. Indentation resilience of conventional and auxetic foams. *J. Cell. Plast.* **1998**, *34*, 231–260. [[CrossRef](#)]
31. Alderson, K.L.; Pickles, A.P.; Neale, P.J.; Evans, K.E. Auxetic polyethylene: The effect of a negative poisson's ratio on hardness. *Acta Metall. Mater.* **1994**, *42*, 2261–2266. [[CrossRef](#)]
32. Alderson, K.L.; Simkins, V.R.; Coenen, V.L.; Davies, P.J.; Alderson, A.; Evans, K.E. How to make auxetic fibre reinforced composites. *Phys. Status Solidi Basic Res.* **2005**, *242*, 509–518. [[CrossRef](#)]
33. Ge, C. A comparative study between felted and triaxial compressed polymer foams on cushion performance. *J. Cell. Plast.* **2013**, *49*, 521–533. [[CrossRef](#)]
34. Cross, T.M.; Hoffer, K.W.; Jones, D.P.; Kirschner, P.B.; Meschter, J.C. Auxetic Structures and Footwear with Soles Having Auxetic Structures. U.S. Patent 2015/0075034 A1, 19 March 2015.
35. Martin, P.G. Filtering Face-Piece Respirator Having an Auxetic Mesh in the Mask Body. U.S. Patent 2011/0155137 A1, 30 June 2011.
36. Wang, Z.; Hu, H. 3D auxetic warp-knitted spacer fabrics. *Phys. Status Solidi Basic Res.* **2014**, *251*, 281–288. [[CrossRef](#)]
37. Sanami, M.; Ravirala, N.; Alderson, K.; Alderson, A. Auxetic materials for sports applications. *Procedia Eng.* **2014**, *72*, 453–458. [[CrossRef](#)]
38. Alderson, A.; Evans, K.E.; Rasburn, J. Separation Process and Apparatus. WO Patent 1999022838A1, 14 May 1999.
39. Alderson, A.; Rasburn, J.; Evans, K.E. An Auxetic Filter: A Tuneable Filter Displaying Enhanced Size Selectivity or Defouling Properties. *Ind. Eng. Chem. Res.* **2000**, *39*, 654–665. [[CrossRef](#)]
40. Alderson, A.; Rasburn, J.; Evans, K.E. Mass transport properties of auxetic (negative Poisson's ratio) foams. *Phys. Status Solidi* **2007**, *244*, 817–827. [[CrossRef](#)]
41. Hou, Y.; Neville, R.; Scarpa, F.; Remillat, C.; Gu, B.; Ruzzene, M. Graded conventional-auxetic Kirigami sandwich structures: Flatwise compression and edgewise loading. *Compos. Part B Eng.* **2014**, *59*, 33–42. [[CrossRef](#)]
42. Hou, Y.; Tai, Y.H.; Lira, C.; Scarpa, F.; Yates, J.R.; Gu, B. The bending and failure of sandwich structures with auxetic gradient cellular cores. *Compos. Part A Appl. Sci. Manuf.* **2013**, *49*, 119–131. [[CrossRef](#)]
43. Hrysomallis, C.; Morrison, W.; He, J. Assessing the shock absorption of thigh pads. *J. Sci. Med.* **1999**, *2*, 49. [[CrossRef](#)]

44. Payne, T.; Mitchell, S.; Halkon, B.; Bibb, R. A systematic approach to the characterisation of human impact injury scenarios in sport. *BMJ Open Sport Exerc. Med.* **2016**, *2*, e000017. [[CrossRef](#)] [[PubMed](#)]
45. Schmikli, S.L.; Backx, F.J.G.; Kemler, H.J.; Van Mechelen, W. National survey on sports injuries in the netherlands: Target populations for sports injury prevention programs. *Clin. J. Sport Med.* **2009**, *19*, 101–106. [[CrossRef](#)] [[PubMed](#)]
46. Statista. Sporting Goods Industry—Statistics & Facts [Internet]. 2018. Available online: <https://www.statista.com/topics/961/sporting-goods/> (accessed on 1 May 2018).
47. Ankrah, S.; Mills, N.J. Analysis of ankle protection in Association football. *Sport Eng.* **2004**, *7*, 41–52. [[CrossRef](#)]
48. Ankrah, S.; Mills, N.J. Performance of football shin guards for direct stud impacts. *Sport Eng.* **2003**, *6*, 207–219. [[CrossRef](#)]
49. Hrysomallis, C. Surrogate thigh model for assessing impact force attenuation of protective pads. *J. Sci. Med. Sport* **2009**, *12*, 35–41. [[CrossRef](#)] [[PubMed](#)]
50. Michel, F.I.; Schmitt, K.U.; Liechti, B.; Stämpfli, R.; Brühwiler, P. Functionality of back protectors in snow sports concerning safety requirements. *Procedia Eng.* **2010**, *2*, 2869–2874. [[CrossRef](#)]
51. Adams, C.; James, D.; Senior, T.; Allen, T.; Hamilton, N. Development of a Method for Measuring Quasi-static Stiffness of Snowboard Wrist Protectors. *Procedia Eng.* **2016**, *147*, 378–383. [[CrossRef](#)]
52. Mills, N.J. The biomechanics of hip protectors. *Proc. Inst. Mech. Eng. Part H* **1996**, *210*, 259–266. [[CrossRef](#)] [[PubMed](#)]
53. Jenkins, M. *Materials in Sports Equipment*; Woodhead Publishing Ltd.: Cambridge, UK, 2007; Volume 2, pp. 138–139.
54. American Society for Testing and Materials. *ASTM F2040-02: Standard Specification for Helmets Used for Recreational Snow Sports*; ASTM International: West Conshohocken, PA, USA, 2002; Volume 15, pp. 1–4.
55. British Standards Institution. *BS 6183-3:2000-Protective Equipment for Cricketers*; British Standards Institution: London, UK, 2000.
56. British Standards Institution. *Helmets for Alpine Skiers and Snowboarders*; BS EN 1077:2007; British Standards Institution: London, UK, 2007; Volume 3.
57. European Committee for Standardization. *Protective Clothing—Shin Guards for Association Football Players—Requirements and Test Methods*; BS EN: 13061:2009; European Committee for Standardization: Brussels, Belgium, 2009.
58. World Fightsport & Martial Arts Council. Official Rulebook. 2010. Available online: www.wfmc-kickboxing.com (accessed on 29 June 2017).
59. Lyn, G.; Mills, N.J. Design of foam crash mats for head impact protection. *Sport. Eng.* **2001**, *4*, 153–163. [[CrossRef](#)]
60. British Standards Institution. *Sports Mats, Part 1: Gymnastic Mats, Safety Requirements*; British Standards Institution: London, UK, 2013.
61. European Committee for Standardization. *Protective Clothing—Wrist, Palm, Knee and Elbow Protectors for Users of Roller Sports Equipment—Requirements and Test Methods*; EN 14120:2003; European Committee for Standardization: Brussels, Belgium, 2003.
62. European Committee for Standardization. *Motorradfahrer Schutzkleidung Teil 2 Rückenprotektoren*; EN 1621-2: 2003; European Committee for Standardization: Brussels, Belgium, 2003.
63. Dickson, T.J.; Trathen, S.; Terwiel, F.A.; Waddington, G.; Adams, R. Head injury trends and helmet use in skiers and snowboarders in Western Canada, 2008–2009 to 2012–2013: An ecological study. *Scand. J. Med. Sci. Sports* **2017**, *27*, 236–244. [[CrossRef](#)] [[PubMed](#)]
64. Ekeland, A.; Rødven, A.; Heir, S. Injury Trends in Recreational Skiers and Boarders in the 16-Year Period 1996–2012. In *Snow Sports Trauma and Safety*; Scher, I.S., Greenwald, R.M., Petrone, N., Eds.; Springer: Cham, Switzerland, 2017; pp. 3–16.
65. Mez, J.; Daneshvar, D.H.; Kiernan, P.T.; Abdolmohammadi, B.; Alvarez, V.E.; Huber, B.R.; Alosco, M.L.; Solomon, T.M.; Nowinski, C.J.; McHale, L.; et al. Clinicopathological Evaluation of Chronic Traumatic Encephalopathy in Players of American Football. *JAMA* **2017**, *318*, 360–370. [[PubMed](#)]
66. King, A.I.; Yang, K.H.; Zhang, L.; Hardy, W.; Viano, D. Is Head Injury Caused by Linear or Angular Acceleration? In Proceedings of the IRCOBI Conference, Lisbon, Portugal, 25–26 September 2003; pp. 1–12.

67. Rowson, S.; Duma, S.M. Brain injury prediction: Assessing the combined probability of concussion using linear and rotational head acceleration. *Ann. Biomed. Eng.* **2013**, *41*, 873–882. [[CrossRef](#)] [[PubMed](#)]
68. National Operating Committee on Standards for Athletic Equipment (NOCSAE). *Standard Test Method and Equipment Used in Evaluating the Performance Characteristics of Protective Headgear/Equipment*; DOC. 001-13m15; NOCSAE: Overland Park, KS, USA, 2011.
69. McIntosh, A.S.; Andersen, T.E.; Bahr, R.; Greenwald, R.; Kleiven, S.; Turner, M.; Varese, M.; McCrory, P. Sports helmets now and in the future. *Br. J. Sports Med.* **2011**, *45*, 1258–1265. [[CrossRef](#)] [[PubMed](#)]
70. Casson, I.R.; Viano, D.C.; Powell, J.W.; Pellman, E.J. Twelve years of National Football League concussion data. *Sports Health* **2010**, *2*, 471–483. [[CrossRef](#)] [[PubMed](#)]
71. British Standards Institution. *Protective Helmets for Vehicle Users*; BS 6658:1985; British Standards Institution: London, UK, 1985.
72. British Standards Institution. *Specification for Head Protectors for Cricketers*; BS 7928:2013; British Standards Institution: London, UK, 2013.
73. McIntosh, A.S.; Janda, D. Evaluation of cricket helmet performance and comparison with baseball and ice hockey helmets. *Br. J. Sports Med.* **2003**, *37*, 325–330. [[CrossRef](#)] [[PubMed](#)]
74. Van Bekkum, J.E.; Williams, J.M.; Morris, P.G. Cycle commuting and perceptions of barriers: Stages of change, gender and occupation. *Health Educ.* **2011**, *111*, 476–497. [[CrossRef](#)]
75. Heinen, E.; Maat, K.; Van Wee, B. The role of attitudes toward characteristics of bicycle commuting on the choice to cycle to work over various distances. *Transp. Res. Part D* **2011**, *16*, 102–109. [[CrossRef](#)]
76. Willinger, R.; Deck, C.; Halldin, P.; Otte, D. Towards advanced bicycle helmet test methods. In Proceedings of the International Cycling Safety Conference, Göteborg, Sweden, 18–19 November 2014; pp. 1–11.
77. Zuzarte, P. Protective Helmet. U.S. Patent 6,658,671 B1, 9 December 2003.
78. Aare, M.; Kleiven, S.; Halldin, P. Injury tolerances for oblique impact helmet testing. *Int. J. Crashworthiness* **2004**, *9*, 15–23. [[CrossRef](#)]
79. Kleiven, S. Influence of impact direction on the human head in prediction of subdural hematoma. *J. Neurotrauma* **2003**, *20*, 365–379. [[CrossRef](#)] [[PubMed](#)]
80. Kleiven, S. Evaluation of head injury criteria using a finite element model validated against experiments on localized brain motion, intracerebral acceleration, and intracranial pressure. *Int. J. Crashworthiness* **2006**, *11*, 65–79. [[CrossRef](#)]
81. Kleiven, S.; Hardy, W.N. Correlation of an FE Model of the Human Head with Local Brain Motion—Consequences for Injury Prediction. *Stapp Car Crash J.* **2002**, *46*, 123–144. [[PubMed](#)]
82. Dura, J.V.; Garcia, A.C.; Solaz, J. Testing shock absorbing materials: The application of viscoelastic linear model. *Sport Eng.* **2002**, *5*, 9–14. [[CrossRef](#)]
83. Hayes, S.G.; Venkatraman, P. *Materials and Technology for Sportswear and Performance Apparel*; CRC Press: Boca Raton, FL, USA, 2016; p. 314.
84. Adams, C.; James, D.; Senior, T.; Allen, T.; Hamilton, N. Effect of surrogate design on the measured stiffness of snowboarding wrist protectors. *Sport Eng.* **2018**, *1*, 1–9.
85. Michel, F.I.; Schmitt, K.U.; Greenwald, R.M.; Russell, K.; Simpson, F.I.; Schulz, D.; Langran, M. White Paper: Functionality and efficacy of wrist protectors in snowboarding-towards a harmonized international standard. *Sport Eng.* **2013**, *16*, 197–210. [[CrossRef](#)]
86. Payne, T.; Mitchell, S.; Halkon, B.; Bibb, R.; Waters, M. Development of a synthetic human thigh impact surrogate for sports personal protective equipment testing. *Proc. Inst. Mech. Eng. Part P* **2016**, *230*, 5–16. [[CrossRef](#)]
87. Petrone, N.; Carraro, G.; Dal Castello, S.; Broggio, L.; Koptuyug, A.; Backstrom, M. A novel instrumented human head surrogate for the impact evaluation of helmets. *Proceedings* **2018**, *2*, 269. [[CrossRef](#)]
88. Nakamura, K.E.N.I.; Wada, M.; Kuga, S.; Okano, T. Poisson's Ratio of Cellulose I β and Cellulose II. *J. Polym. Sci. Part B Polym. Phys.* **2004**, *42*, 1206–1211. [[CrossRef](#)]
89. Caddock, B.D.; Evans, K.E. Microporous materials with negative Poisson's ratios. I. Microstructure and mechanical properties. *J. Phys. D. Appl. Phys.* **1989**, *22*, 1877–1882. [[CrossRef](#)]
90. Dominec, J.; Vase, P.; Svoboda, P.; Plechacek, V.; Laermans, C. Elastic Moduli for Three Superconducting Phases of Bi-Sr-Ca-Cu-O. *Mod. Phys. Lett. B* **1992**, *6*, 1049. [[CrossRef](#)]
91. Baughman, R.H.; Shacklette, J.M.; Zakhidov, A.A.; Stafstro, S. Negative Poisson's ratios as a common feature of Cubic Metals. *Nature* **1998**, *392*, 362–365. [[CrossRef](#)]

92. Clarke, J.F.; Duckett, R.A.; Hine, P.J.; Hutchinson, I.J.; Ward, I.M. Negative Poisson's ratios in angle-ply laminates: Theory and experiment. *Composites* **1994**, *25*, 863–868. [[CrossRef](#)]
93. Barthelat, F.; Tang, H.; Zavattieri, P.D.; Li, C.M.; Espinosa, H.D. On the mechanics of mother-of-pearl: A key feature in the material hierarchical structure. *J. Mech. Phys. Solids* **2007**, *55*, 306–337. [[CrossRef](#)]
94. Rad, M.S.; Mohsenizadeh, S.; Ahmad, Z. Finite element approach and mathematical formulation of viscoelastic auxetic honeycomb structures for impact mitigation. *J. Eng. Sci. Technol.* **2017**, *12*, 471–490.
95. Gibson, L.J.; Ashby, M.F.; Schajer, G.S.; Robertson, C.I. The mechanics of two-dimensional cellular materials. *Proc. R. Soc. Lond. A* **1982**, *382*, 25–42. [[CrossRef](#)]
96. Masters, I.G.; Evans, K.E. Models for the elastic deformation of honeycombs. *Compos. Struct.* **1996**, *35*, 403–422. [[CrossRef](#)]
97. Whitty, J.P.M.; Nazare, F.; Alderson, A. Modelling the effects of density variations on the in-plane Poisson's ratios and Young's moduli of periodic conventional and re-entrant honeycombs—Part 1: Rib thickness variations. *Cell. Polym.* **2002**, *21*, 69–98.
98. Nkansah, M.A.; Evans, K.E.; Hutchinson, I.J. Modelling the mechanical properties of an auxetic molecular network. *Model. Simul. Mater. Sci. Eng.* **1994**, *2*, 337–352. [[CrossRef](#)]
99. Strek, T.; Maruszewski, B.; Narojczyk, J.W.; Wojciechowski, K.W. Finite element analysis of auxetic plate deformation. *J. Non-Cryst. Solids* **2008**, *354*, 4475–4480. [[CrossRef](#)]
100. Ge, Z.; Hu, H.; Liu, Y. A finite element analysis of a 3D auxetic textile structure for composite reinforcement. *Smart Mater. Struct.* **2013**, *22*, 84005. [[CrossRef](#)]
101. Zhang, J.; Lu, G.; Wang, Z.; Ruan, D.; Alomarah, A.; Durandet, Y. Large deformation of an auxetic structure in tension: Experiments and finite element analysis. *Compos. Struct.* **2018**, *184*, 92–101. [[CrossRef](#)]
102. Almgren, R.F. An isotropic three-dimensional structure with Poisson's ratio = -1 . *J. Elast.* **1985**, *15*, 427–430.
103. Wojciechowski, K.W. Constant thermodynamic tension Monte Carlo studies of elastic properties of a two-dimensional system of hard cyclic hexamers. *Mol. Phys.* **1987**, *61*, 1247–1258. [[CrossRef](#)]
104. Prall, D.; Lakes, R.S. Properties of A Chiral Honeycomb with A Poisson's Ratio of -1 . *Int. J. Mech. Sci.* **1997**, *39*, 305–314. [[CrossRef](#)]
105. Grima, J.N.; Evans, K.E. Auxetic behavior from rotating squares. *J. Mater. Sci. Lett.* **2000**, *19*, 1563–1565. [[CrossRef](#)]
106. Grima, J.N.; Alderson, A.; Evans, K.E. Auxetic behaviour from rotating rigid units. *Phys. Status Solidi Basic Res.* **2005**, *242*, 561–575. [[CrossRef](#)]
107. Grima, J.N.; Farrugia, P.S.; Gatt, R.; Zammit, V. Connected Triangles Exhibiting Negative Poisson's Ratios and Negative Thermal Expansion. *J. Phys. Soc. Jpn.* **2007**, *76*, 025001. [[CrossRef](#)]
108. Attard, D.; Grima, J.N. A three-dimensional rotating rigid units network exhibiting negative Poisson's ratios. *Phys. Status Solidi Basic Res.* **2012**, *249*, 1330–1338. [[CrossRef](#)]
109. Grima, J.N.; Gatt, R.; Ravirala, N.; Alderson, A.; Evans, K.E. Negative Poisson's ratios in cellular foam materials. *Mater. Sci. Eng. A* **2006**, *423*, 214–218. [[CrossRef](#)]
110. Smith, C.W.; Grima, J.N.; Evans, K.E. Novel mechanism for generating auxetic behaviour in reticulated foams: Missing rib foam model. *Acta Mater.* **2000**, *48*, 4349–4356. [[CrossRef](#)]
111. Bertoldi, K. Harnessing Instabilities to Design Tunable Architected Cellular Materials. *Annu. Rev. Mater. Res.* **2017**, *47*, 51–61. [[CrossRef](#)]
112. Alderson, A.; Evans, K.E. Modelling concurrent deformation mechanisms in auxetic microporous polymers. *J. Mater. Sci.* **1997**, *32*, 2797–2809. [[CrossRef](#)]
113. Bertoldi, K.; Reis, P.M.; Willshaw, S.; Mullin, T. Negative poisson's ratio behavior induced by an elastic instability. *Adv. Mater.* **2010**, *22*, 361–366. [[CrossRef](#)] [[PubMed](#)]
114. Overvelde, J.T.B.; Shan, S.; Bertoldi, K. Compaction through buckling in 2D periodic, soft and porous structures: Effect of pore shape. *Adv. Mater.* **2012**, *24*, 2337–2342. [[CrossRef](#)] [[PubMed](#)]
115. Overvelde, J.T.B.; Bertoldi, K. Relating pore shape to the non-linear response of periodic elastomeric structures. *J. Mech. Phys. Solids* **2014**, *64*, 351–366. [[CrossRef](#)]
116. Babaei, S.; Shim, J.; Weaver, J.C.; Chen, E.R.; Patel, N.; Bertoldi, K. 3D soft metamaterials with negative poisson's ratio. *Adv. Mater.* **2013**, *25*, 5044–5049. [[CrossRef](#)] [[PubMed](#)]
117. Javid, F.; Smith-Roberge, E.; Innes, M.C.; Shanian, A.; Weaver, J.C.; Bertoldi, K. Dimpled elastic sheets: A new class of non-porous negative Poisson's ratio materials. *Sci. Rep.* **2015**, *5*, 1–9. [[CrossRef](#)] [[PubMed](#)]

118. Gibson, L.J.; Ashby, M.F. *Cellular Solids. Structure and Properties*; Cambridge University Press: Cambridge, UK, 1997; pp. 67, 176–183, 259–264, 286, 498.
119. Choi, J.B.; Lakes, R.S. Analysis of elastic modulus of conventional foams and of re-entrant foam materials with a negative Poisson's ratio. *Int. J. Mech. Sci.* **1995**, *37*, 51–59. [[CrossRef](#)]
120. Evans, K.E.; Alderson, A.; Christian, F.R. Auxetic Two-dimensional Polymer Networks. *J. Chem. Soc. Faraday Trans.* **1995**, *91*, 2671–2680. [[CrossRef](#)]
121. Alipour, M.M.; Shariyat, M. Analytical zigzag formulation with 3D elasticity corrections for bending and stress analysis of circular/annular composite sandwich plates with auxetic cores. *Compos. Struct.* **2015**, *132*, 175–197. [[CrossRef](#)]
122. Wu, W.; Song, X.; Liang, J.; Xia, R.; Qian, G.; Fang, D. Mechanical properties of anti-tetrachiral auxetic stents. *Compos. Struct.* **2018**, *185*, 381–392. [[CrossRef](#)]
123. Abramovitch, H.; Burgard, M.; Edery-Azulay, L.; Evans, K.E.; Hoffmeister, M.; Miller, W.; Scarpa, F.; Smith, C.W.; Tee, K.F. Smart tetrachiral and hexachiral honeycomb: Sensing and impact detection. *Compos. Sci. Technol.* **2010**, *70*, 1072–1079. [[CrossRef](#)]
124. Grima, J.N.; Attard, D.; Ellul, B.; Gatt, R. An improved analytical model for the elastic constants of auxetic and conventional hexagonal honeycombs. *Cell. Polym.* **2011**, *30*, 287–310.
125. Hughes, T.P.; Marmier, A.; Evans, K.E. Auxetic frameworks inspired by cubic crystals. *Int. J. Solids Struct.* **2010**, *47*, 1469–1476. [[CrossRef](#)]
126. Wang, X.T.; Li, X.W.; Ma, L. Interlocking assembled 3D auxetic cellular structures. *Mater. Des.* **2016**, *99*, 467–476. [[CrossRef](#)]
127. Zhang, J.; Lu, G.; Ruan, D.; Wang, Z. Tensile behavior of an auxetic structure: Analytical modeling and finite element analysis. *Int. J. Mech. Sci.* **2018**, *136*, 143–154. [[CrossRef](#)]
128. Dirrenberger, J.; Forest, S.; Jeulin, D. Elastoplasticity of auxetic materials. *Comput. Mater. Sci.* **2012**, *64*, 57–61. [[CrossRef](#)]
129. Najarian, F.; Alipour, R.; Shokri Rad, M.; Nejad, A.F.; Razavykia, A. Multi-objective optimization of converting process of auxetic foam using three different statistical methods. *Meas. J. Int. Meas. Confed.* **2018**, *119*, 108–116. [[CrossRef](#)]
130. Evans, K.E.; Nkansah, M.A.; Hutchinson, I.J. Auxetic Foams: Modelling Negative Poisson's Ratios. *Acta Metall. Mater.* **1994**, *42*, 1289–1294. [[CrossRef](#)]
131. Crespo, J.; Montáns, F.J. A continuum approach for the large strain finite element analysis of auxetic materials. *Int. J. Mech. Sci.* **2018**, *135*, 441–457. [[CrossRef](#)]
132. Ciambella, J.; Bezazi, A.; Saccomandi, G.; Scarpa, F. Nonlinear elasticity of auxetic open cell foams modeled as continuum solids. *J. Appl. Phys.* **2015**, *117*, 184902. [[CrossRef](#)]
133. Lee, J.; Choi, J.B.; Choi, K. Application of homogenization FEM analysis to regular and re-entrant honeycomb structures. *J. Mater. Sci.* **1996**, *31*, 4105–4110. [[CrossRef](#)]
134. Huang, F.-Y.; Yan, B.-H.; Yang, D.U. The effects of material constants on the micropolar elastic honeycomb structure with negative Poisson's ratio using the finite element method. *Eng. Comput.* **2002**, *19*, 742–763. [[CrossRef](#)]
135. Yang, D.U.; Lee, S.; Huang, F.Y. Geometric effects on micropolar elastic honeycomb structure with negative Poisson's ratio using the finite element method. *Finite Elem. Anal. Des.* **2003**, *39*, 187–205.
136. Liu, W.; Wang, N.; Huang, J.; Zhong, H. The effect of irregularity, residual convex units and stresses on the effective mechanical properties of 2D auxetic cellular structure. *Mater. Sci. Eng. A* **2014**, *609*, 26–33. [[CrossRef](#)]
137. Yang, C.; Vora, H.D.; Chang, Y.B. Application of Auxetic Polymeric Structures for Body Protection. In Proceedings of the ASME 2016 Conference on Smart Materials, Adaptive Structures & Intelligent Systems, Stowe, VT, USA, 28–30 September 2016; pp. 1–5.
138. Streck, T.; Jopek, H.; Idczak, E.; Wojciechowski, K.W. Computational modelling of structures with non-intuitive behaviour. *Materials* **2017**, *10*, 1386. [[CrossRef](#)] [[PubMed](#)]
139. Bezazi, A.; Scarpa, F.; Remillat, C. A novel centresymmetric honeycomb composite structure. *Compos. Struct.* **2005**, *71*, 356–364. [[CrossRef](#)]
140. Mousanezhad, D.; Ebrahimi, H.; Haghpanah, B.; Ghosh, R.; Ajdari, A.; Hamouda, A.M.S.; Vaziri, A. Spiderweb honeycombs. *Int. J. Solids Struct.* **2015**, *66*, 218–227. [[CrossRef](#)]

141. Grima, J.N.; Cauchi, R.; Gatt, R.; Attard, D. Honeycomb composites with auxetic out-of-plane characteristics. *Compos. Struct.* **2013**, *106*, 150–159. [[CrossRef](#)]
142. Silva, T.A.A.; Panzera, T.H.; Brandão, L.C.; Lauro, C.H.; Boba, K.; Scarpa, F. Preliminary investigations on auxetic structures based on recycled rubber. *Phys. Status Solidi Basic Res.* **2012**, *249*, 1353–1358. [[CrossRef](#)]
143. Milton, G.W. Composite materials with poisson's ratios close to—1. *J. Mech. Phys. Solids* **1992**, *40*, 1105–1137. [[CrossRef](#)]
144. Evans, K.E.; Nkansah, M.A.; Hutchinson, I.J. Modelling Negative Poisson Ratio Effects in Network-Embedded Composites. *Acta Metall. Mater.* **1992**, *40*, 2463–2469. [[CrossRef](#)]
145. Streck, T.; Jopek, H.; Maruszewski, B.T.; Nienartowicz, M. Computational analysis of sandwich-structured composites with an auxetic phase. *Phys. Status Solidi Basic Res.* **2014**, *251*, 354–366. [[CrossRef](#)]
146. Streck, T.; Jopek, H.; Nienartowicz, M. Dynamic response of sandwich panels with auxetic cores. *Phys. Status Solidi Basic Res.* **2015**, *252*, 1540–1550. [[CrossRef](#)]
147. Poźniak, A.A.; Wojciechowski, K.W.; Grima, J.N.; Mizzi, L. Planar auxeticity from elliptic inclusions. *Compos. Part B Eng.* **2016**, *94*, 379–388. [[CrossRef](#)]
148. Streck, T.; Jopek, H.; Idczak, E. Computational design of two-phase auxetic structures. *Phys. Status Solidi Basic Res.* **2016**, *253*, 1387–1394. [[CrossRef](#)]
149. Jopek, H.; Stręk, T. Thermoauxetic behavior of composite structures. *Materials* **2018**, *11*, 294. [[CrossRef](#)] [[PubMed](#)]
150. Jopek, H.; Streck, T. Thermal and structural dependence of auxetic properties of composite materials. *Phys. Status Solidi Basic Res.* **2015**, *252*, 1551–1558. [[CrossRef](#)]
151. Doyoyo, M.; Wan Hu, J. Plastic failure analysis of an auxetic foam or inverted strut lattice under longitudinal and shear loads. *J. Mech. Phys. Solids* **2006**, *54*, 1479–1492. [[CrossRef](#)]
152. Qiao, J.X.; Chen, C.Q. Impact resistance of uniform and functionally graded auxetic double arrowhead honeycombs. *Int. J. Impact Eng.* **2015**, *83*, 47–58. [[CrossRef](#)]
153. Qiao, J.; Chen, C.Q. Analyses on the In-Plane Impact Resistance of Auxetic Double Arrowhead Honeycombs. *J. Appl. Mech.* **2015**, *82*, 51007. [[CrossRef](#)]
154. Lu, Z.; Wang, Q.; Li, X.; Yang, Z. Elastic properties of two novel auxetic 3D cellular structures. *Int. J. Solids Struct.* **2017**, *124*, 46–56. [[CrossRef](#)]
155. Shufrin, I.; Pasternak, E.; Dyskin, A.V. Negative Poisson's ratio in hollow sphere materials. *Int. J. Solids Struct.* **2015**, *54*, 192–214. [[CrossRef](#)]
156. Spadoni, A.; Ruzzene, M. Elasto-static micropolar behavior of a chiral auxetic lattice. *J. Mech. Phys. Solids* **2012**, *60*, 156–171. [[CrossRef](#)]
157. Qi, C.; Remennikov, A.; Pei, L.Z.; Yang, S.; Yu, Z.H.; Ngo, T.D. Impact and close-in blast response of auxetic honeycomb-cored sandwich panels: Experimental tests and numerical simulations. *Compos. Struct.* **2017**, *180*, 161–178. [[CrossRef](#)]
158. Wang, X.T.; Wang, B.; Li, X.W.; Ma, L. Mechanical properties of 3D re-entrant auxetic cellular structures. *Int. J. Mech. Sci.* **2017**, *131*, 396–407. [[CrossRef](#)]
159. Ranga, D.; Strangwood, M. Finite element modelling of the quasi-static and dynamic behaviour of a solid sports ball based on component material properties. *Procedia Eng.* **2010**, *2*, 3287–3292. [[CrossRef](#)]
160. Jiang, L.; Hu, H. Low-velocity impact response of multilayer orthogonal structural composite with auxetic effect. *Compos. Struct.* **2017**, *169*, 62–68. [[CrossRef](#)]
161. Miller, W.; Smith, C.W.; Scarpa, F.; Evans, K.E. Flatwise buckling optimization of hexachiral and tetrachiral honeycombs. *Compos. Sci. Technol.* **2010**, *70*, 1049–1056. [[CrossRef](#)]
162. Novak, N.; Vesenjaj, M.; Ren, Z. Computational Simulation and Optimization of Functionally Graded Auxetic Structures Made from Inverted Tetrapods. *Phys. Status Solidi Basic Res.* **2017**, *254*, 1–7. [[CrossRef](#)]
163. Safikhani Nasim, M.; Etemadi, E. Three dimensional modeling of warp and woof periodic auxetic cellular structure. *Int. J. Mech. Sci.* **2018**, *136*, 475–481. [[CrossRef](#)]
164. Carta, G.; Brun, M.; Baldi, A. Design of a porous material with isotropic negative Poisson's ratio. *Mech. Mater.* **2016**, *97*, 67–75. [[CrossRef](#)]
165. Scarpa, F.; Blain, S.; Lew, T.; Perrott, D.; Ruzzene, M.; Yates, J.R. Elastic buckling of hexagonal chiral cell honeycombs. *Compos. Part A Appl. Sci. Manuf.* **2007**, *38*, 280–289. [[CrossRef](#)]
166. Wang, Z.; Hu, H. A finite element analysis of an auxetic warp-knitted spacer fabric structure. *Text. Res. J.* **2015**, *85*, 404–415. [[CrossRef](#)]

167. Gao, Q.; Wang, L.; Zhou, Z.; Ma, Z.D.; Wang, C.; Wang, Y. Theoretical, numerical and experimental analysis of three-dimensional double-V honeycomb. *Mater. Des.* **2018**, *139*, 380–391. [CrossRef]
168. Farhan, M.; Shahid, M. Negative Poissons ratio behavior of idealized elastomeric auxetic cellular structures for various carbon black nanoparticles loadings. *J. Elastomers Plast.* **2015**, *47*, 479–487. [CrossRef]
169. Javadi, A.A.; Faramarzi, A.; Farmani, R. Design and optimization of microstructure of auxetic materials. *Eng. Comput.* **2012**, *29*, 260–276. [CrossRef]
170. Lee, D.; Shin, S. Evaluation of Optimized Topology Design of Cross-Formed Structures with a Negative Poisson's Ratio. *Iran. J. Sci. Technol. Trans. Civ. Eng.* **2016**, *40*, 109–120. [CrossRef]
171. Vogiatzis, P.; Chen, S.; Wang, X.; Li, T.; Wang, L. Topology optimization of multi-material negative Poisson's ratio metamaterials using a reconciled level set method. *Comput. Aided Des.* **2017**, *83*, 15–32. [CrossRef]
172. Ren, X.; Shen, J.; Tran, P.; Ngo, T.D.; Xie, Y.M. Design and characterisation of a tuneable 3D buckling-induced auxetic metamaterial. *Mater. Des.* **2018**, *139*, 336–342. [CrossRef]
173. Li, H.; Luo, Z.; Gao, L.; Walker, P. Topology optimization for functionally graded cellular composites with metamaterials by level sets. *Comput. Methods Appl. Mech. Eng.* **2017**, *328*, 340–364. [CrossRef]
174. Qin, H.; Yang, D.; Ren, C. Modelling theory of functional element design for metamaterials with arbitrary negative Poisson's ratio. *Comput. Mater. Sci.* **2018**, *150*, 121–133. [CrossRef]
175. Yang, S.; Qi, C.; Guo, D.M.; Wang, D. Energy absorption of an re-entrant honeycombs with negative Poisson's ratio. *Appl. Mech. Mater.* **2012**, *148*, 992–995. [CrossRef]
176. Hou, X.; Deng, Z.; Zhang, K. Dynamic Crushing Strength Analysis of Auxetic Honeycombs. *Acta Mech. Solida Sin.* **2016**, *29*, 490–501. [CrossRef]
177. Wang, Y.; Wang, L.; Ma, Z.D.; Wang, T. A negative Poisson's ratio suspension jounce bumper. *Mater. Des.* **2016**, *103*, 90–99. [CrossRef]
178. Imbalzano, G.; Tran, P.; Ngo, T.D.; Lee, P.V.S. Three-dimensional modelling of auxetic sandwich panels for localised impact resistance. *J. Sandw. Struct. Mater.* **2017**, *19*, 291–316. [CrossRef]
179. Imbalzano, G.; Tran, P.; Ngo, T.D.; Lee, P.V.S. A numerical study of auxetic composite panels under blast loadings. *Compos. Struct.* **2016**, *135*, 339–352. [CrossRef]
180. Critchley, R.; Corni, I.; Stokes, K.; Walsh, F.C.; Wharton, J.; Wood, R.J.K. High Strain Materials for Body Armour Inspired from Nature High Strain Materials for Body Armour Inspired from Nature. 2014. Available online: <https://www.researchgate.net/publication/267261907> (accessed on 4 June 2018).
181. Bryson, A.; Smith, L. Impact response of sports materials. *Procedia Eng.* **2010**, *2*, 2961–2966. [CrossRef]
182. Mills, N.J.; Gilchrist, A. Oblique impact testing of bicycle helmets. *Int. J. Impact Eng.* **2008**, *35*, 1075–1086. [CrossRef]
183. Scarpa, F.; Giacomini, J.; Zhang, Y.; Pastorino, P. Mechanical performance of auxetic polyurethane foam for antivibration glove applications. *Cell. Polym.* **2005**, *24*, 253–268.
184. Choi, J.B.; Lakes, R.S. Nonlinear Analysis of the Poisson's Ratio of Negative Poisson's Ratio Foams. *J. Compos. Mater.* **1994**, *29*, 113–128. [CrossRef]
185. Chan, N.; Evans, K.E. Fabrication methods for auxetic foams. *J. Mater. Sci.* **1997**, *32*, 5945–5953. [CrossRef]
186. Loureiro, M.A.; Lakes, R.S. Scale-up of transformation of negative Poisson's ratio foam: Slabs. *Cell. Polym.* **1997**, *16*, 349–363.
187. Bianchi, M.; Scarpa, F.; Banse, M.; Smith, C.W. Novel generation of auxetic open cell foams for curved and arbitrary shapes. *Acta Mater.* **2011**, *59*, 686–691. [CrossRef]
188. Allen, T.; Hewage, T.; Newton-Mann, C.; Wang, W.; Duncan, O.; Alderson, A. Fabrication of Auxetic Foam Sheets for Sports Applications. *Phys. Status Solidi Basic Res.* **2017**, *254*, 1700596. [CrossRef]
189. Choi, J.B.; Lakes, R.S. Nonlinear properties of polymer cellular materials with a negative Poisson's ratio. *Mater. Sci.* **1992**, *27*, 4678–4684. [CrossRef]
190. Alderson, A.; Davies, P.J.; Alderson, K.; Smart, G.M. The Effects of Processing on the Topology and Mechanical Properties of Negative Poisson's Ratio Foams. In Proceedings of the 2005 ASME International Mechanical Engineering Congress and Exposition, Orlando, FL, USA, 5–11 November 2005; pp. 1–8.
191. Gatt, R.; Attard, D.; Manicaro, E.; Chetcuti, E.; Grima, J.N. On the effect of heat and solvent exposure on the microstructure properties of auxetic foams: A preliminary study. *Phys. Status Solidi Basic Res.* **2011**, *248*, 39–44. [CrossRef]
192. Bianchi, M.; Frontoni, S.; Scarpa, F.; Smith, C.W. Density change during the manufacturing process of PU-PE open cell auxetic foams. *Phys. Status Solidi Basic Res.* **2011**, *248*, 30–38. [CrossRef]

193. Scarpa, F.; Pastorino, P.; Garelli, A.; Patsias, S.; Ruzzene, M. Auxetic compliant flexible PU foams: Static and dynamic properties. *Phys. Status Solidi Basic Res.* **2005**, *242*, 681–694. [\[CrossRef\]](#)
194. Duncan, O.; Allen, T.; Foster, L.; Gatt, R.; Grima, J.N.; Alderson, A. Controlling Density and Modulus in Auxetic Foam Fabrications—Implications for Impact and Indentation Testing. *Proceedings* **2018**, *2*, 250. [\[CrossRef\]](#)
195. Boba, K.; Bianchi, M.; McCombe, G.; Gatt, R.; Griffin, A.C.; Richardson, R.M.; Scarpa, F.; Hamerton, I.; Grima, J. Blocked shape memory effect in negative Poisson's ratio polymer metamaterials. *ACS Appl. Mater. Interfaces* **2016**, *8*, 20319–20328. [\[CrossRef\]](#) [\[PubMed\]](#)
196. Grima, J.N.; Attard, D.; Gatt, R.; Cassar, R.N. A novel process for the manufacture of auxetic foams and for their re-conversion to conventional form. *Adv. Eng. Mater.* **2009**, *11*, 533–535. [\[CrossRef\]](#)
197. Lowe, A.; Lakes, R.S. Negative Poisson's ratio foam as seat cushion material. *Cell. Polym.* **2000**, *19*, 157–167.
198. Chan, N.; Evans, K.E. Microscopic examination of the microstructure and deformation of conventional and auxetic foams. *J. Mater. Sci.* **1997**, *2*, 5725–5736. [\[CrossRef\]](#)
199. Martz, E.O.; Lee, T.; Lakes, R.S.; Goel, V.K.; Park, J.B. Re-entrant transformation methods in closed cell foams. *Cell. Polym.* **1996**, *15*, 229–249.
200. Quadri, F.; Bellisario, D.; Ciampoli, L.; Costanza, G.; Santo, L. Auxetic epoxy foams produced by solid state foaming. *J. Cell. Plast.* **2015**, *52*, 441–454. [\[CrossRef\]](#)
201. Xu, T.; Li, G. A shape memory polymer based syntactic foam with negative Poisson's ratio. *Mater. Sci. Eng. A* **2011**, *528*, 6804–6811. [\[CrossRef\]](#)
202. Wang, K.; Chang, Y.H.; Chen, Y.; Zhang, C.; Wang, B. Designable dual-material auxetic metamaterials using three-dimensional printing. *Mater. Des.* **2015**, *67*, 159–164. [\[CrossRef\]](#)
203. McDonald, S.A.; Ravirala, N.; Withers, P.J.; Alderson, A. In situ three-dimensional X-ray microtomography of an auxetic foam under tension. *Scr. Mater.* **2009**, *60*, 232–235. [\[CrossRef\]](#)
204. Lisiecki, J.; Klysz, S.; Blazejewicz, T.; Gmurczyk, G.; Reymer, P. Tomographic examination of auxetic polyurethane foam structures. *Phys. Status Solidi Basic Res.* **2013**, *251*, 314–320. [\[CrossRef\]](#)
205. American Society for Testing and Materials. *ASTM-D412-15a: Standard Test Methods for Vulcanized Rubber and Thermoplastic Elastomers—Tension*; ASTM International: West Conshohocken, PA, USA, 2015; Volume 9, pp. 1–14.
206. Miller, W.; Hook, P.B.; Smith, C.W.; Wang, X.; Evans, K.E. The manufacture and characterisation of a novel, low modulus, negative Poisson's ratio composite. *Compos. Sci. Technol.* **2009**, *69*, 651–655. [\[CrossRef\]](#)
207. Miller, W.; Ren, Z.; Smith, C.W.; Evans, K.E. A negative Poisson's ratio carbon fibre composite using a negative Poisson's ratio yarn reinforcement. *Compos. Sci. Technol.* **2012**, *72*, 761–766. [\[CrossRef\]](#)
208. Bhattacharya, S.; Zhang, G.H.; Ghita, O.; Evans, K.E. The variation in Poisson's ratio caused by interactions between core and wrap in helical composite auxetic yarns. *Compos. Sci. Technol.* **2014**, *102*, 87–93. [\[CrossRef\]](#)
209. Zhang, G.; Ghita, O.R.; Evans, K.E. Dynamic thermo-mechanical and impact properties of helical auxetic yarns. *Compos. Part B Eng.* **2016**, *99*, 494–505. [\[CrossRef\]](#)
210. Zhang, G.H.; Ghita, O.; Evans, K.E. The fabrication and mechanical properties of a novel 3-component auxetic structure for composites. *Compos. Sci. Technol.* **2015**, *117*, 257–267. [\[CrossRef\]](#)
211. Zhang, G.; Ghita, O.R.; Lin, C.; Evans, K.E. Large-scale manufacturing of helical auxetic yarns using a novel semi-coextrusion process. *Text. Res. J.* **2017**, 1–12. [\[CrossRef\]](#)
212. Ge, Z.; Hu, H.; Liu, S. A novel plied yarn structure with negative Poisson's ratio. *J. Text. Inst.* **2016**, *107*, 578–588. [\[CrossRef\]](#)
213. Lim, T.C. Semi-auxetic yarns. *Phys. Status Solidi Basic Res.* **2014**, *251*, 273–280. [\[CrossRef\]](#)
214. Liu, S.; Pan, X.; Zheng, D.; Du, Z.; Liu, G.; Yang, S. Study on the structure formation and heat treatment of helical auxetic complex yarn. *Text. Res. J.* **2018**. [\[CrossRef\]](#)
215. Sloan, M.R.; Wright, J.R.; Evans, K.E. The helical auxetic yarn—A novel structure for composites and textiles; Geometry, manufacture and mechanical properties. *Mech. Mater.* **2011**, *43*, 476–486. [\[CrossRef\]](#)
216. McAfee, J.; Faisal, N.H. Parametric sensitivity analysis to maximise auxetic effect of polymeric fibre based helical yarn. *Compos. Struct.* **2017**, *162*, 1–12. [\[CrossRef\]](#)
217. Wright, J.R.; Burns, M.K.; James, E.; Sloan, M.R.; Evans, K.E. On the design and characterisation of low-stiffness auxetic yarns and fabrics. *Text. Res. J.* **2012**, *82*, 645–654. [\[CrossRef\]](#)
218. Alderson, K.L.; Alderson, A.; Smart, G.; Simkins, V.R.; Davies, P.J. Auxetic polypropylene fibres: Part 1—Manufacture and characterisation. *Plast Rubber Compos.* **2002**, *31*, 344–349. [\[CrossRef\]](#)

219. Ravirala, N.; Alderson, A.; Alderson, K.L.; Davies, P.J. Auxetic polypropylene films. *Polym. Eng. Sci.* **2005**, *45*, 517–528. [[CrossRef](#)]
220. Alderson, A.; Alderson, K. Expanding materials and applications: Exploiting auxetic textiles. *Tech. Text. Int.* **2005**, *14*, 29–34.
221. Simkins, V.R.; Alderson, A.; Davies, P.J.; Alderson, K.L. Single fibre pullout tests on auxetic polymeric fibres. *J. Mater. Sci.* **2005**, *40*, 4355–4364. [[CrossRef](#)]
222. Ng, W.S.; Hu, H. Woven fabrics made of auxetic plied yarns. *Polymers* **2018**, *10*, 226.
223. Alderson, A. *Smart Solutions from Auxetic Materials*; Med-Tech Innovation: Chester, UK, 2011.
224. Verma, P.; Shofner, M.L.; Lin, A.; Wagner, K.B.; Griffin, A.C. Induction of auxetic response in needle-punched nonwovens: Effects of temperature, pressure, and time. *Phys. Status Solidi* **2016**, *253*, 1270–1278. [[CrossRef](#)]
225. Verma, P.; Shofner, M.L.; Lin, A.; Wagner, K.B.; Griffin, A.C. Inducing out-of-plane auxetic behavior in needle-punched nonwovens. *Phys. Status Solidi Basic Res.* **2015**, *252*, 1455–1464. [[CrossRef](#)]
226. Zulifqar, A.; Hua, T.; Hu, H. Development of UNI-stretch woven fabrics with zero and negative Poisson's ratio. *Text. Res. J.* **2017**. [[CrossRef](#)]
227. Alderson, K.; Alderson, A.; Anand, S.; Simkins, V.; Nazare, S.; Ravirala, N. Auxetic warp knit textile structures. *Phys. Status Solidi Basic Res.* **2012**, *249*, 1322–1329. [[CrossRef](#)]
228. Ma, P.; Chang, Y.; Jiang, G. Design and fabrication of auxetic warp-knitted structures with a rotational hexagonal loop. *Text. Res. J.* **2016**, *86*, 2151–2157. [[CrossRef](#)]
229. Ugbohue, S.C.; Kim, Y.K.; Warner, S.B.; Fan, Q.; Yang, C.L.; Kyzymchuk, O.; Feng, Y.; Lord, J. The formation and performance of auxetic textiles. Part II: Geometry and structural properties. *J. Text. Inst.* **2011**, *102*, 424–433. [[CrossRef](#)]
230. Wang, Z.; Hu, H.; Xiao, X. Deformation behaviors of three-dimensional auxetic spacer fabrics. *Text. Res. J.* **2014**, *84*, 1361–1372. [[CrossRef](#)]
231. Wang, Z.; Hu, H. Tensile and forming properties of auxetic warp-knitted spacer fabrics. *Text. Res. J.* **2017**, *87*, 1925–1937. [[CrossRef](#)]
232. Chang, Y.; Ma, P. Fabrication and property of auxetic warp-knitted spacer structures with mesh. *Text. Res. J.* **2017**. [[CrossRef](#)]
233. Chang, Y.; Ma, P.; Jiang, G. Energy absorption property of warp-knitted spacer fabrics with negative Poisson's ratio under low velocity impact. *Compos. Struct.* **2017**, *182*, 471–477. [[CrossRef](#)]
234. Chang, Y.; Ma, P. Energy absorption and Poisson's ratio of warp-knitted spacer fabrics under uniaxial tension. *Text. Res. J.* **2018**. [[CrossRef](#)]
235. Hu, H.; Wang, Z.; Liu, S. Development of auxetic fabrics using flat knitting technology. *Text. Res. J.* **2011**, *81*, 1493–1502.
236. Steffens, F.; Oliveira, F.R.; Mota, C.; Figueiro, R. High-performance composite with negative Poisson's ratio. *J. Mater. Res.* **2017**, *32*, 3477–3484. [[CrossRef](#)]
237. Goto, K.; Arai, M.; Matsuda, T.; Kubo, G. Elasto-viscoplastic analysis for negative through-the-thickness Poisson's ratio of woven laminate composites based on homogenization theory. *Int. J. Mech. Sci.* **2017**. [[CrossRef](#)]
238. Ge, Z.; Hu, H.; Liu, Y. Numerical analysis of deformation behavior of a 3D textile structure with negative Poisson's ratio under compression. *Text. Res. J.* **2015**, *85*, 548–557. [[CrossRef](#)]
239. Ge, Z.; Hu, H. A theoretical analysis of deformation behavior of an innovative 3D auxetic textile structure. *J. Text. Inst.* **2015**, *106*, 101–109. [[CrossRef](#)]
240. Nava-Gómez, G.G.; Camacho-Montes, H.; Sabina, F.J.; Rodríguez-Ramos, R.; Fuentes, L.; Guinovart-Díaz, R. Elastic properties of an orthotropic binary fiber-reinforced composite with auxetic and conventional constituents. *Mech. Mater.* **2012**, *48*, 1–25. [[CrossRef](#)]
241. Liaqat, M.; Samad, H.A.; Hamdani, S.T.A.; Nawab, Y. The development of novel auxetic woven structure for impact applications. *J. Text. Inst.* **2017**, *108*, 1264–1270. [[CrossRef](#)]
242. American Society for Testing and Materials. *D6110-17: Standard Test Method for Determining the Charpy Impact Resistance of Notched Specimens of Plastics*; ASTM International: West Conshohocken, PA, USA, 2010; pp. 1–17.
243. Zhou, L.; Jiang, L.; Hu, H. Auxetic composites made of 3D textile structure and polyurethane foam. *Phys. Status Solidi Basic Res.* **2016**, *257*, 1331–1341. [[CrossRef](#)]
244. Jiang, L.; Gu, B.; Hu, H. Auxetic composite made with multilayer orthogonal structural reinforcement. *Compos. Struct.* **2016**, *135*, 23–29. [[CrossRef](#)]

245. Wang, Z.; Hu, H. Auxetic materials and their potential applications in textiles. *Text. Res. J.* **2014**, *84*, 1600–1611. [[CrossRef](#)]
246. Ma, P.; Chang, Y.; Boakye, A.; Jiang, G. Review on the knitted structures with auxetic effect. *J. Text. Inst.* **2017**, *108*, 947–961. [[CrossRef](#)]
247. Yuan, S.; Shen, F.; Bai, J.; Chua, C.K.; Wei, J.; Zhou, K. 3D soft auxetic lattice structures fabricated by selective laser sintering: TPU powder evaluation and process optimization. *Mater. Des.* **2017**, *120*, 317–327. [[CrossRef](#)]
248. Lantada, A.D.; De Blas Romero, A.; Schwentenwein, M.; Jellinek, C.; Homa, J. Lithography-based ceramic manufacture (LCM) of auxetic structures: Present capabilities and challenges. *Smart Mater. Struct.* **2016**, *25*, 054015. [[CrossRef](#)]
249. Critchley, B.R.; Corni, I.; Wharton, J.A.; Walsh, F.C.; Wood, R.J.K.; Stokes, K.R. The Preparation of Auxetic Foams by Three-Dimensional Printing and Their Characteristics. *Adv. Eng. Mater.* **2013**, *15*, 980–985. [[CrossRef](#)]
250. Hengsbach, S.; Lantada, A.D. Direct laser writing of auxetic structures: Present capabilities and challenges. *Smart Mater. Struct.* **2014**, *23*, 085033. [[CrossRef](#)]
251. Yang, L.; Harrysson, O.; West, H.; Cormier, D. Mechanical properties of 3D re-entrant honeycomb auxetic structures realized via additive manufacturing. *Int. J. Solids Struct.* **2015**, *69*, 475–490. [[CrossRef](#)]
252. Li, T.; Wang, L. Bending behavior of sandwich composite structures with tunable 3D-printed core materials. *Compos. Struct.* **2017**, *175*, 46–57. [[CrossRef](#)]
253. Li, D.; Ma, J.; Dong, L.; Lakes, R.S. Stiff square structure with a negative Poisson's ratio. *Mater. Lett.* **2017**, *188*, 149–151. [[CrossRef](#)]
254. Ma, Q.; Peel, L.D. Development of spiral auxetic structures. *Compos. Struct.* **2018**, *192*, 310–316. [[CrossRef](#)]
255. Boldrin, L.; Hummel, S.; Scarpa, F.; Di Maio, D.; Lira, C.; Ruzzene, M.; Remillat, C.; Lim, T.; Rajasekaran, R.; Patsias, S. Dynamic behaviour of auxetic gradient composite hexagonal honeycombs. *Compos. Struct.* **2016**, *149*, 114–124. [[CrossRef](#)]
256. Huang, H.H.; Wong, B.L.; Chou, Y.C. Design and properties of 3D-printed chiral auxetic metamaterials by reconfigurable connections. *Phys. Status Solidi Basic Res.* **2016**, *253*, 1557–1564. [[CrossRef](#)]
257. Saxena, K.K.; Calius, E.P.; Das, R. Tailoring Cellular Auxetics For Wearable Applications with Multimaterial 3D Printing. In Proceedings of the ASME 2016 International Mechanical Engineering Congress & Exposition, Phoenix, AZ, USA, 11–17 November 2016.
258. Saxena, K.K.; Das, R.; Calius, E.P. 3D printable multimaterial cellular auxetics with tunable stiffness. *arXiv* **2017**, arXiv:1707.04486.
259. Jiang, Y.; Li, Y. Novel 3D-Printed Hybrid Auxetic Mechanical Metamaterial with Chirality-Induced Sequential Cell Opening Mechanisms. *Adv. Eng. Mater.* **2018**, *20*, 1–9. [[CrossRef](#)]
260. Jiang, Y.; Li, Y. 3D Printed Auxetic Mechanical Metamaterial with Chiral Cells and Re-entrant Cores. *Sci. Rep.* **2018**, *8*, 2397. [[CrossRef](#)] [[PubMed](#)]
261. Brighenti, R. Smart behaviour of layered plates through the use of auxetic materials. *Thin-Walled Struct.* **2014**, *84*, 432–442. [[CrossRef](#)]
262. Ingrole, A.; Hao, A.; Liang, R. Design and modeling of auxetic and hybrid honeycomb structures for in-plane property enhancement. *Mater. Des.* **2017**, *117*, 72–83. [[CrossRef](#)]
263. Li, X.; Lu, Z.; Yang, Z.; Yang, C. Directions dependence of the elastic properties of a 3D augmented re-entrant cellular structure. *Mater. Des.* **2017**, *134*, 151–162. [[CrossRef](#)]
264. Zhang, X.; Yang, D. Mechanical properties of auxetic cellular material consisting of re-entrant hexagonal honeycombs. *Materials* **2016**, *9*, 900. [[CrossRef](#)] [[PubMed](#)]
265. Li, D.; Dong, L.; Lakes, R.S. A unit cell structure with tunable Poisson's ratio from positive to negative. *Mater. Lett.* **2016**, *164*, 456–459. [[CrossRef](#)]
266. Ebrahimi, H.; Mousanezhad, D.; Nayeb-Hashemi, H.; Norato, J.; Vaziri, A. 3D cellular metamaterials with planar anti-chiral topology. *Mater. Des.* **2018**, *145*, 226–231. [[CrossRef](#)]
267. Fu, M.; Liu, F.; Hu, L. A novel category of 3D chiral material with negative Poisson's ratio. *Compos. Sci. Technol.* **2018**, *160*, 111–118. [[CrossRef](#)]
268. Hanifpour, M.; Petersen, C.F.; Alava, M.J.; Zapperi, S. Mechanics of disordered auxetic metamaterials. *arXiv* **2017**, arXiv:1704.00943.

269. Yang, C.; Vora, H.D.; Chang, Y.B. Evaluation of Auxetic Polymeric Structures for Use in Protective Pads. In Proceedings of the ASME 2016 International Mechanical Engineering Congress & Exposition, Phoenix, AZ, USA, 11–17 November 2016.
270. Yang, C.; Vora, H.; Chang, Y. Behavior of Auxetic Structures Under Compression and Impact Forces. *Smart Mater. Struct.* **2017**, *27*, 025012. [[CrossRef](#)]
271. Bates, S.R.G.; Farrow, I.R.; Trask, R.S. 3D printed polyurethane honeycombs for repeated tailored energy absorption. *Mater. Des.* **2016**, *112*, 172–183. [[CrossRef](#)]
272. Alderson, A.; Alderson, K.L.; McDonald, S.A.; Mottershead, B.; Nazare, S.; Withers, P.J.; Yao, Y. Piezomorphic materials. *Macromol. Mater. Eng.* **2013**, *298*, 318–327. [[CrossRef](#)]
273. Zorzetto, L.; Ruffoni, D. Re-entrant inclusions in cellular solids: From defects to reinforcements. *Compos. Struct.* **2017**, *176*, 195–204. [[CrossRef](#)]
274. Lakes, R.S.; Elms, K. Indentability of conventional and negative Poisson's ratio foams. *J. Compos. Mater.* **1993**, *27*, 1193–1202. [[CrossRef](#)]
275. Scarpa, F.; Yates, J.R.; Ciffo, L.G.; Patsias, S. Dynamic crushing of auxetic open-cell polyurethane foam. *Proc. Inst. Mech. Eng. Part C* **2002**, *216*, 1153–1156. [[CrossRef](#)]
276. Bocquet, C. Bra with Variable-Volume Straps. WO Patent 2006045935A, 4 May 2006.
277. Timishenko, S.P.; Goodier, J.N. *Theory of Elasticity*, 3rd ed.; McGraw-Hill: New York, NY, USA, 1970.
278. Budynas, R.G. *Advanced Strength and Applied Stress Analysis*; WCB/McGraw-Hill: New York, NY, USA, 1999; pp. 21, 80.
279. Roark, R.J.; Young, W.C. *Formulas for Stress and Strain*; McGraw-Hill: New York, NY, USA, 2012; pp. 20–22, 48–50.
280. Lempriere, B.M. Poisson's ratio in orthotropic materials. *AIAA J.* **1968**, *6*, 2226–2227. [[CrossRef](#)]
281. Wojciechowski, K.W. Remarks on "Poisson ratio beyond the limits of the elasticity theory". *J. Phys. Soc. Jpn.* **2003**, *72*, 1819–1820. [[CrossRef](#)]
282. Lakes, R.S. Design Considerations for Materials with Negative Poisson's Ratios. *J. Mech. Des.* **1993**, *115*, 696. [[CrossRef](#)]
283. Alderson, K.L.; Fitzgerald, A.; Evans, K.E. The strain dependent indentation resilience of auxetic microporous polyethylene. *J. Mater. Sci.* **2000**, *35*, 4039–4047. [[CrossRef](#)]
284. Lin, D.C.; Shreiber, D.I.; Dimitriadis, E.K.; Horkay, F. Spherical indentation of soft matter beyond the Hertzian regime: Numerical and experimental validation of hyperelastic models. *Biomech. Model. Mechanobiol.* **2009**, *8*, 345–358. [[CrossRef](#)] [[PubMed](#)]
285. Argatov, I.I.; Guinovart-Díaz, R.; Sabina, F.J. On local indentation and impact compliance of isotropic auxetic materials from the continuum mechanics viewpoint. *Int. J. Eng. Sci.* **2012**, *54*, 42–57. [[CrossRef](#)]
286. Wang, Y.C.; Lakes, R. Analytical parametric analysis of the contact problem of human buttocks and negative Poisson's ratio foam cushions. *Int. J. Solids Struct.* **2002**, *39*, 4825–4838. [[CrossRef](#)]
287. Waters, N.E. The indentation of thin rubberer sheets by cylindrical indetors. *Br. J. Appl. Phys.* **1965**, *16*, 1387–1392. [[CrossRef](#)]
288. Photiou, D.; Sarris, E.; Constantinides, G. On the conical indentation response of elastic auxetic materials: Effects of Poisson's ratio, contact friction and cone angle. *Int. J. Solids Struct.* **2017**, *1*, 33–42. [[CrossRef](#)]
289. Photiou, D.; Sarris, E.; Constantinides, G. Erratum to "On the conical indentation response of elastic auxetic materials: Effects of Poisson's ratio, contact friction and cone angle" [Int. J. Solids Struct. 81 (2016) 33–42]. *Int. J. Solids Struct.* **2017**, *110–111*, 404. [[CrossRef](#)]
290. Guo, X.; Jin, F.; Gao, H. Mechanics of non-slipping adhesive contact on a power-law graded elastic half-space. *Int. J. Solids Struct.* **2011**, *48*, 2565–2575. [[CrossRef](#)]
291. Li, S.; Al-Badani, K.; Gu, Y.; Lake, M.; Li, L.; Rothwell, G.; Ren, J. The Effects of Poisson's Ratio on the Indentation Behavior of Materials with Embedded System in an Elastic Matrix. *Phys. Status Solidi Basic Res.* **2017**, *254*, 1–8. [[CrossRef](#)]
292. Aw, J.; Zhao, H.; Norbury, A.; Li, L.; Rothwell, G.; Ren, J. Effects of Poisson's ratio on the deformation of thin membrane structures under indentation. *Phys. Status Solidi Basic Res.* **2015**, *252*, 1526–1532. [[CrossRef](#)]
293. Morris, D.J.; Cook, R.F. Indentation fracture of low-dielectric constant films: Part II. Indentation fracture mechanics model. *J. Mater. Res.* **2008**, *23*, 2429–2442. [[CrossRef](#)]
294. Argatov, I.I.; Sabina, F.J. Small-scale indentation of an elastic coated half-space: The effect of compliant substrate. *Int. J. Eng. Sci.* **2016**, *104*, 87–96. [[CrossRef](#)]

295. Chan, N.; Evans, K.E. The mechanical properties of conventional and auxetic foams. Part I: Compression and tension. *J. Cell. Plast.* **1999**, *35*, 130–165. [[CrossRef](#)]
296. Adam, M.M.; Berger, J.R.; Martin, P.A. Singularities in auxetic elastic bimetals. *Mech. Res. Commun.* **2013**, *47*, 102–105. [[CrossRef](#)]
297. Kwon, K.; Phan, A.V. Symmetric-Galerkin boundary element analysis of the dynamic T-stress for the interaction of a crack with an auxetic inclusion. *Mech. Res. Commun.* **2015**, *69*, 91–96. [[CrossRef](#)]
298. Song, F.; Zhou, J.; Xu, X.; Xu, Y.; Bai, Y. Effect of a negative poisson ratio in the tension of ceramics. *Phys. Rev. Lett.* **2008**, *100*, 1–4. [[CrossRef](#)] [[PubMed](#)]
299. Mohsenizadeh, S.; Alipour, R.; Shokri Rad, M.; Farokhi Nejad, A.; Ahmad, Z. Crashworthiness assessment of auxetic foam-filled tube under quasi-static axial loading. *Mater. Des.* **2015**, *88*, 258–268. [[CrossRef](#)]
300. Bezazi, A.; Scarpa, F. Mechanical behaviour of conventional and negative Poisson's ratio thermoplastic polyurethane foams under compressive cyclic loading. *Int. J. Fatigue*. **2007**, *29*, 922–930. [[CrossRef](#)]
301. Pastorino, P.; Scarpa, F.; Patsias, S.; Yates, J.R.; Haake, S.J.; Ruzzene, M. Strain rate dependence of stiffness and Poisson's ratio of auxetic open cell PU foams. *Phys. Status Solidi Basic Res.* **2007**, *244*, 955–965. [[CrossRef](#)]
302. Nakonieczna, P.; Wierzbicki, Ł.; Śladowska, B.; Leonowicz, M.; Lisiecki, J. Composites with Impact Absorption Ability Based on Shear Thickening Fluids and Auxetic Foams. *Compos. Theory Pract.* **2017**, *2*, 67–72.
303. Qi, C.; Yang, S.; Wang, D.; Yang, L.J. Ballistic resistance of honeycomb sandwich panels under in-plane high-velocity impact. *Sci. World J.* **2013**, *2013*, 892781. [[CrossRef](#)] [[PubMed](#)]
304. Liu, W.; Wang, N.; Luo, T.; Lin, Z. In-plane dynamic crushing of re-entrant auxetic cellular structure. *Mater. Des.* **2016**, *100*, 84–91. [[CrossRef](#)]
305. Yang, S.; Chalivendra, V.B.; Kim, Y.K. Impact behaviour of auxetic Kevlar®/epoxy composites. *IOP Conf. Ser. Mater. Sci. Eng.* **2017**, *254*, 042031. [[CrossRef](#)]
306. Yang, S.; Chalivendra, V.B.; Kim, Y.K. Fracture and impact characterization of novel auxetic Kevlar®/Epoxy laminated composites. *Compos. Struct.* **2017**, *168*, 120–129. [[CrossRef](#)]
307. Alderson, K.L.; Coenen, V.L. The low velocity impact response of auxetic carbon fibre laminates. *Phys. Status Solidi* **2008**, *245*, 489–496. [[CrossRef](#)]
308. Coenen, V.L.; Alderson, K.L. Mechanisms of failure in the static indentation resistance of auxetic carbon fibre laminates. *Phys. Status Solidi Basic Res.* **2011**, *248*, 66–72. [[CrossRef](#)]
309. International Organization for Standardization. *Mechanical Vibration and Shock—Hand-Arm Vibration—Method for Measuring the Vibration Transmissibility of Resilient Materials When Loaded by the Hand-Arm System*; ISO 13753:1999; ISO: Geneva, Switzerland, 1999.
310. Chen, C.P.; Lakes, R.S. Dynamic wave dispersion and loss properties of conventional and negative Poisson's ratio polymeric cellular materials. *Cell. Polym.* **1989**, *8*, 343–369.
311. Lisiecki, J.; Nowakowski, D.; Reymer, P. Fatigue Properties of Polyurethane Foams, With Special Emphasis on Auxetic Foams, Used for Helicopter Pilot Seat Cushion Inserts. *Fatigue Aircr. Struct.* **2014**, *1*, 72–78. [[CrossRef](#)]
312. Evans, K.E. The design of doubly curved sandwich panels with honeycomb cores. *Compos. Struct.* **1991**, *17*, 95–111. [[CrossRef](#)]
313. Alderson, A.; Alderson, K.L.; Chirima, G.; Ravirala, N.; Zied, K.M. The in-plane linear elastic constants and out-of-plane bending of 3-coordinated ligament and cylinder-ligament honeycombs. *Compos. Sci. Technol.* **2010**, *70*, 1034–1041. [[CrossRef](#)]
314. Mehta, R. A nose for auxetics. *Mater. World* **2010**, *18*, 9–12.
315. Bianchi, M.; Scarpa, F.; Smith, C.W.; Whittell, G.R. Physical and thermal effects on the shape memory behaviour of auxetic open cell foams. *J. Mater. Sci.* **2010**, *45*, 341–347. [[CrossRef](#)]
316. Allen, T.; Martinello, N.; Zampieri, D.; Hewage, T.; Senior, T.; Foster, L.; Alderson, A. Auxetic foams for sport safety applications. *Procedia Eng.* **2015**, *112*, 104–109. [[CrossRef](#)]
317. Lim, T.C.; Alderson, A.; Alderson, K.L. Experimental studies on the impact properties of auxetic materials. *Phys. Status Solidi*. **2014**, *251*, 307–313. [[CrossRef](#)]
318. D3O. Trust Helmet Pad System [Internet]. Web Page. 2018. Available online: <https://www.d3o.com/products/trust-helmet-pad-system/> (accessed on 25 January 2018).

319. Xu, K.; Tan, Y.; Xin, J.H.; Liu, Y.; Lu, C.; Deng, Y.; Han, C.; Hu, H.; Wang, P. A novel impact hardening polymer with negative Poisson's ratio for impact protection. *Mater. Today Commun.* **2015**, *5*, 50–59. [[CrossRef](#)]
320. Foster, L.; Peketi, P.; Allen, T.; Senior, T.; Duncan, O.; Alderson, A. Application of Auxetic Foam in Sports Helmets. *Appl. Sci.* **2018**, *8*, 354. [[CrossRef](#)]



© 2018 by the authors. Licensee MDPI, Basel, Switzerland. This article is an open access article distributed under the terms and conditions of the Creative Commons Attribution (CC BY) license (<http://creativecommons.org/licenses/by/4.0/>).